Structure–Reactivity: Comparison between the Carbonation of Epoxidized Vegetable Oils and the Corresponding Epoxidized Fatty Acid Methyl Ester

Xiaoshuang Cai, Manoelito Matos, Sébastien Leveneur

Structure-reactivity: comparison between the carbonation of epoxidized vegetable oils and the corresponding epoxidized fatty acid methyl ester

*Xiaoshuang Cai[a], Manoelito Matos[a], Sébastien Leveneur[a,b]**

[a]Normandie Univ, INSA Rouen, UNIROUEN, LSPC - Laboratoire de sécurité des procédés chimiques, EA4704, 76000 Rouen, France.

[b]Laboratory of Industrial Chemistry and Reaction Engineering, Process Chemistry Centre, Åbo Akademi University, Biskopsgatan 8, FI-20500 Åbo/Turku, Finland.

Corresponding author:

E-mail address:

Xiaoshuang Cai: xiaoshuang.cai@insa-rouen.fr

Manoelito Matos: manoelito.matos@insa-rouen.fr

Sébastien Leveneur: sebastien.leveneur@insa-rouen.fr , Tel: +33 2 32 95 66 54; Fax: +33 2 32 95 66 52

ABSTRACT

Vegetable oils are renewable biomass that can substitute fossil raw materials for sustainable development. These oils are made of different types of fatty acids (building-blocks), which could lead to different reactivity towards chemical reaction.

In order to investigate the correlation between reactivity and structure of vegetable oils, we have compared the reactivity of epoxidized cottonseed oil (ECSO) and its epoxidized fatty acid methyl ester (EFAME) towards carbonation reaction by using homogeneous catalyst tetra-butylammonium bromide (TBABr). Mass transfer and physicochemical properties were determined and further applied to estimate the intrinsic rate constants during the kinetic modeling stage.

It was found that density for both systems was similar, but the difference of viscosity was important. Mass transfer coefficients were similar for the carbonated species, but the ones of EFAME and FAME were found to be ca. 100 times lower than ECSO and CSO. The solubility of CO_2 was found to be higher in FAME-derivatives than in CSO-derivatives. We have found that the rate constant of carbonation of EFAME can be 1.4 times higher than the one of ECSO. A linear relationship between the carbonation rate constant of epoxidized vegetable oil and its fatty acid methyl ester with temperature was found.

Keywords: Carbonation; Epoxidized Vegetable Oil; Physicochemical Property; Structure Reactivity; Kinetic Modeling

1. Introduction

Nowadays, renewable biomass is more and more used in industry, such as fat,[1] vegetable oil,[2] wood, [3] etc. The use of biomass as raw materials in chemical industry involves several challenges, e.g., gather of crop, fluctuations in biomass production, pretreatment of biomass. Besides, the chemical contents of biomass depend on the species, location or season. The development of kinetic and thermodynamic models, which are needed for the design and optimization of the production, becomes complicated.

Even though these biomass have complex chemical structures, the building-blocks are similar, for example, fatty acids for vegetable oils, amino-acids for proteins and cellulose, hemicellulose, lignin for wood. In the case of vegetable oils, would it be possible to predict the intrinsic kinetics of these complex chemical structures by knowing the intrinsic kinetics of their building-blocks? In other words, what is the relationship between the structure and reactivity?

During the last decades, vegetable oil has become a popular alternative feedstock for producing petroleum-substitutes, since it is renewable, biodegradable, relatively inexpensive and eco-friendly.[4] As a chemical platform, vegetable oils can be valorized through chemical modification into variety of products or intermediate materials, including polymers, composites, emulsions, coatings, binders in ink formulations, gels.[5]

Transesterification of vegetable oils (soybean oil, palm oil, cottonseed oil, sunflower oil, rapeseed oil, etc.) is the most common way to be used for biodiesel production.[6–8] Some literature reviews have been published on the main technologies of transesterification process. [9,10] In this process procedure, triglycerides are transformed into fatty acid methyl ester with acid/base/enzyme heterogeneous catalysts or under supercritical conditions. [11–14] Hydrochloric

acid, sulfuric or sulfonic acids and carboxylates have been used as acid catalysts, while base catalysts, i.e., sodium/potassium hydroxide and solid basic metal oxides are generally applied.[15] Also, several studies have proved that transesterification process helps to decrease the viscosity of vegetable oils, which is 9 to 17 times of fatty acid methyl esters and affects mass transfer.[16–18]

Epoxidized vegetable oils are popular and more desirable for industrial development currently.[19–21] They have been widely and strongly encouraged to be applied in chemical industry, such as plasticizers and stabilizers for environmentally friendly polymers, additives for lubricant, and precursors or intermediates for urethane, etc. [22–25] Indeed, epoxidation of vegetable oils by Prileschajew method is a complex system involving several exothermic reaction steps and phases.[26-30]

In 2015, Huang et al. [31] have studied the epoxidation of different fatty acid methyl esters, and have demonstrated that the kinetics of epoxidation and ring-opening increases with the number of unsaturated groups.

In 2016, Omonov et al.[32] have compared the kinetics of epoxidation of canola oil and its transesterified form. They have found that the kinetics of epoxidation of the transesterified form was faster, but they did not take into account the mass transfer, difference of viscosity and different side reactions. Indeed in 2018, Cai et al. [33] have shown that side reactions of ring opening can be due to different nucleophiles (water, hydrogen peroxide and acetic and peracetic acids).

In 2018, Adriana et al. [34] have investigated the epoxidation of oleic acid and cottonseed oil catalyzed by cation exchange resin of Amberlite IR-120.

To the best of our knowledge, no one has performed a fair comparison between the kinetics of vegetable oil and their corresponding fatty acid methyl ester.

The objective of this study is to measure the difference of reactivity between a biomass macromolecule, i.e., triglyceride, and its constituting elements, i.e., fatty acids. For that, the carbonation of epoxidized vegetable oils by using homogeneous catalyst, namely tetra-butylammonium bromide (TBABr), was tested.[35-36] A comparison between the reactivity of epoxidized cottonseed oil and its fatty acid methyl ester counterpart was done. Indeed, the reactive centers, i.e., epoxide groups, are more accessible for epoxidized fatty acid methyl esters than for the corresponding vegetable oils.

Carbonation reaction was chosen because the reactants and products are thermally stable during the storage and loading.[22] This reaction is important for the production of polyurethane by non-isocyanate route.[38] This eco-friendly route consists of the reaction between the cyclic-carbonate and a diamine.

To carry out such study, it is compulsory to take into account the mass transfer phenomena of carbon dioxide from gas to liquid phase. This phenomenon is interfered by the physicochemical properties of the reaction mixture.[36] The structure of the paper is as follows: 1) Comparison of the physicochemical properties; 2) Comparison of mass transfer phenomenon and 3) Comparison of the kinetics.

2. Experimental section

2.1. Materials and Chemicals

Refined cottonseed oil was purchased from ThermoFisher Scientific GmbH (Schwerte, Germany). Formic acid (purity>99 %), hydrogen peroxide (33 wt % in water) and chloroform were obtained from VWR International SAS (Fontenay-sous-Bois, France). Tetra-n-butylammonium bromide (TBABr, purity > 98 %), tetraethylammonium bromide (TEAB, 98 %), and 0.1 mol.L^{-1} of perchloric acid standardized solution in acetic acid were obtained from Alfa Aesar (Alfa Aesar GmbH & Co., Ward Hill, MA, USA). Solution of 0.1 mol.L^{-1} of iodine according HANUS was obtained from Chem-Lab NV (Chem-Lab, Belgium). Solution of 0.1 mol.L^{-1} of sodium thiosulfate was purchased from Sigma-Aldrich (Sigma Aldrich Chemical Co, USA).

2.2. Apparatus and Experimental Procedures

2.2.1. Transesterification of cottonseed oil: preparation of cottonseed oil fatty acid methyl ester (FAME)

Transesterification of cottonseed oil was carried out as described by Campanella, *et al*., [27] with slightly modification. The methanol-catalyst mixture was preheated before being fed and reacted with the cottonseed oil at 70 °C in the reactor. The molar stoichiometry is 6.6:1 (methanol: cottonseed oil) in the presence of 1.0 wt % of NaOH catalyst. The transesterification reaction lasted for 1 hour. After the reaction phase was stratified into two phases, the glycerol phase was removed. The methyl ester phase left in the reactor was washed with 600 mL of distilled water with one drop of phosphoric acid, then, washed three times with

distilled. The product was evaporated using an IKA RV10 control vacuum rotary evaporator (VWR, Darmstadt, Germany) at 60 °C and dried over magnesium sulfate. The resulting product was kept at 3 °C under argon atmosphere.

2.2.2. Epoxidation of cottonseed oil (CSO) and fatty acid methyl ester (FAME)

Epoxidized cottonseed oil and epoxidized fatty acid methyl ester were prepared in a 500 mL glass-jacketed reactor (Figure 1), equipped with a pitched blade impeller (diameter 3.8 cm and 4 blades), a reflux condenser and a thermostatic circulator water bath. A dosing pump was applied for solution injection and metering.

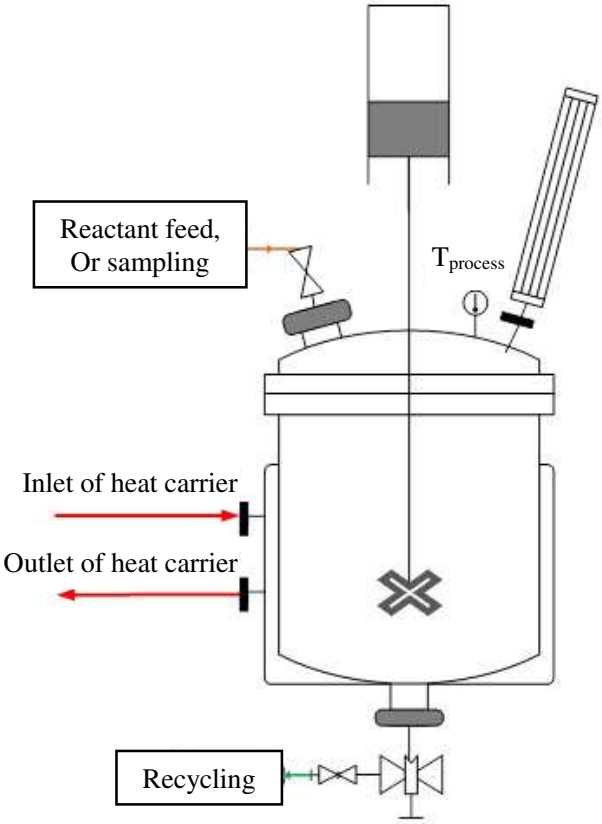

Figure 1. Schematic diagram of epoxidation setup

Preparation of epoxidized cottonseed oil (ECSO)

The preparation of epoxidized cottonseed oil (ECSO) was described as,[30,39] 180.0 g of cottonseed oil and hydrogen peroxide, 50.0 g of distilled water were mixed and preheated in the glass-jacket reactor at 60 °C. Then, 2.9 $mL.min^{-1}$ of formic acid was introduced via a dosing pump for 25 min. The reaction time lasted for 1 hour. After the reaction phase was stratified into two phases, the aqueous phase was removed. The organic phase left in the reactor was washed with 300 mL of Na_2CO_3 (10 wt % in water), followed by being washed three times with 600 mL of distilled water to remove the residual sodium salt. The purified product was evaporated at 60 °C and dried over magnesium sulfate. The resulting epoxidized cottonseed oil was kept at 3 °C under an argon atmosphere. This product had a conversion exceeding 97 % and a selectivity exceeding 81 %.

Preparation of epoxidized cottonseed oil fatty acid methyl ester (EFAME)

For the preparation of EFAME, it was prepared as follows: 100.0 g of cottonseed oil fatty acid methyl ester (FAME), 150.0 g of hydrogen peroxide and 20.0 g of distilled water were mixed and preheated in the glass-jacket reactor at 40 °C. Then, 2.1 $mL.min^{-1}$ of formic acid was introduced via a dosing pump for 20 min. The reaction lasted 2 hours. After the reaction phase was stratified into two phases, the organic phase was separated and washed with 300 mL of Na_2CO_3 (5 wt % in water) and pure distilled water remove the residual acid and salt. The purified product was evaporated at 60 °C and dried over magnesium sulfate. The resulting epoxidized fatty acid methyl ester was kept at 3 °C under an argon atmosphere. This product had a conversion exceeding 90.20 % and a selectivity exceeding 90.59 %.

2.2.3. Carbonation of epoxidized cottonseed oil (ECSO) and epoxidized fatty acid methyl ester (EFAME)

A high-pressure stainless-steel autoclave (Parr Instrument Company, Moline, 300 mL) equipped with a hollow-shaft gas entrainment impeller (diameter 2.5 cm) and a temperature control system was selected for the carbonation (Figure 2). A gas feed system including a CO_2 bottle and a gas reservoir was connected to the reactor. A gas monitoring system equipped with temperature and pressure probes inside the gas reservoir was connected to a computer. The uncertainty for the pressure probe was 0.01 bars and that for the temperature probe was 0.1 °C.

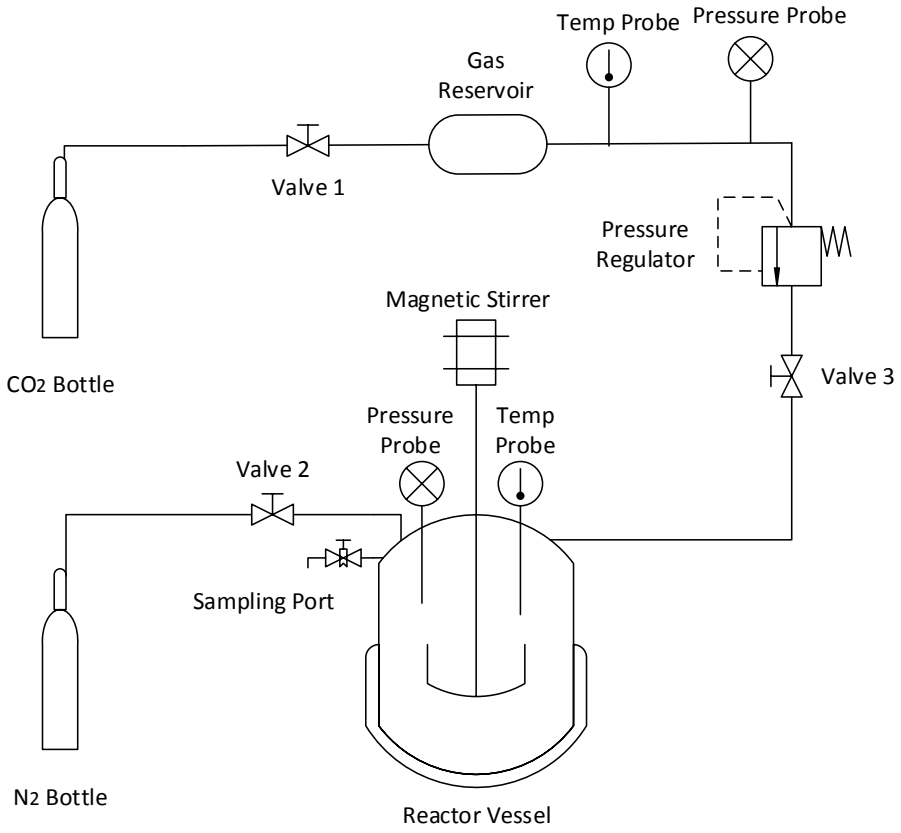

Figure 2. Schematic diagram of carbonation setup

2.3 Analytical methods

2.3.1. Physicochemical properties measurement

In the first stage, physicochemical properties (density and viscosity) measurement of fatty acid methyl ester, and the epoxidized, carbonated derivatives was done.

Density was measured using a digital glass vibrating-tube densitometer (DMA5000, Anton Paar Ltd, Herts, UK) with an accuracy of 1×10^{-3} kg.m^{-3} and 0.001 K for the temperature according to the manufacturer.

Dynamic viscosity of cottonseed oil and its epoxidized, carbonated derivatives were described in our previous work.[35] The dynamic viscosity of cottonseed oil fatty acid methyl ester and its epoxidized, carbonated derivatives were carried out in a digital rolling-ball viscometer (Lovis 2000 ME, Anton Paar, Graz, Austria) with an accuracy of 0.5 % and 0.002 °C for the temperature according to the manufacturer.

Each oil sample was measured three times. The uncertainty of the measurement was evaluated with the standard deviation of the mean s(θ_{mean}), which was calculated as

$$s(\theta_{mean}) = \frac{s(\theta)}{\sqrt{N}} \times 100\% \quad (1)$$

where, s(θ) is the standard deviation of the single value and N is the numbers of experimental points.

2.3.2. Determination of the fatty acid methyl ester components

For determining the fatty acid methyl ester components, a Bruker Scion GC436 gas chromatography, equipped with a split injector and an elastic quartz capillary column (ZB-5, Phenomenex, 30 m × 0.32 mm i.d., 0.25 μm film thickness), was applied. Helium (99.99 %) was used as carrier gas at a constant flow rate of 1.0 mL.min^{-1}. The temperature of the injector was 300 °C. The oven temperature was programmed as 40 °C for 2 min duration and then

increased to 300 °C at 8.0 °C.min^{-1} heating rate and maintained for 34.5 min. The injection volume was 1.0 μL and the split mode was 30:1. All data acquisition and analysis were performed using the Compass CDS software (Agilent Technologies, version 3.0). Table 1 showed brief information about the fatty acid components of cottonseed oil.

The transesterification of components in oil sample was performed as follows: 0.1 mL of the oil sample (4 mg.mL^{-1} in methanol) was sampling into a 10 mL glass vial. Then, 2.5 mL of toluene-methanol mixture (volume fraction 20 %), 0.1 mL of C_{15} internal standard solution (pentadecanoic ethyl ester, 1 mg.mL^{-1} of in methanol) and 0.2 mL of acethyl chloride (purity > 98 %) were added to the vial. The mixture was pretreated at 80 °C for 1 hour before 4.0 mL of sodium carbonate solution (6 wt % in water) and 2.0 mL of toluene were added. The final mixture was vortexed for 5 minutes and the upper layer was further analyzed by GC.

Table 1. Fatty acid components of cottonseed oil [30]

Fatty acid	*C:D* [a]	mass fraction (%)
Linoleic acid	18:2	57.51
Oleic acid	18:1	13.27
Stearic acid	18:0	0.89
Palmitic acid	16:0	28.33

[a] The ratio of the total amount of carbon atoms of the fatty acid to the number of double bond; *C*, Carbon atoms; *D*, Double bond.

2.3.3. Determination of epoxide content

Epoxide content was titrated by the method of Jay.[40] Briefly, 0.100 g of oil sample or organic phase (±0.001 g) was weighted out and dissolved in 10 mL of chloroform, followed by addition

of 20 wt % (in acetic acid) tetraethylammonium bromide (10 mL). Then, the mixture was titrated by 0.1 mol.L^{-1} of perchloric acid standardized solution with a TIM-840 automatic titrator (Radiometer Analytical, France).

2.3.4. Determination of double bond

Double bonds were titrated as described in the Hanus iodine monobromide method,[41] with some modifications. Briefly, 0.200 g of oil sample or organic phase (± 0.001g) was dissolved in 10 mL of chloroform and 10 mL of HANUS (0.1 mol.L^{-1}, iodine solution according HANUS). The mixture was kept in dark place for 1 h. Then, 10 mL of potassium iodide aqueous solution (10 wt %) and 100 mL of water were added for titration with 0.1 mol.L^{-1} sodium thiosulfate solution.

2.3.5. Kinetic study of carbonation reaction

Measurement of CO_2 Solubility

The solubility measurement of CO_2 was conducted in the high-pressure autoclave. During the mass transfer experiments, 90.0 g of oil sample (FAME, EFAME or CFAME) was weighted out and mixed in the reactor, then heated to a desired temperature. The atmosphere inside the reactor was purged with CO_2 for two times. The CO_2 pressure in the reactor was maintained constant by the pressure regulator. When the pressure is stable, the agitation was started at 500 rpm. The values (temperature and pressure) inside the gas reservoir were simultaneously monitored. Table S1 shows the experimental matrix for the mass transfer study.

Carbonation kinetic of epoxidized cottonseed oil (ECSO) and epoxidized fatty acid methyl ester (EFAME)

Carbonation of ECSO and EFAME were carried out as follows:[36,39] epoxidized cottonseed oil (or epoxidized fatty acid methyl ester) and the catalyst TBABr were weighted out in the reactor. The reactor was purged with N_2 for two times followed by heated up to the desired temperature. Then, the atmosphere inside reactor was purged with CO_2 for two times and kept under the desired pressure. After the pressure and temperature were stabilized, the agitation started at 500 rpm. Sample was withdrawn at 1 hour intervals via the sampling port. Table S2 displays the experimental matrix for the carbonation reaction.

Results and discussion

3.1. Comparison of physicochemical properties

The evolutions of density and viscosity of the different compounds with temperature are displayed in Figures S1-S2.[35] Figure S1 shows that as functional groups are big, density is higher, i.e., $\rho_{Carb}>\rho_{Ep}>\rho_{VO}$.

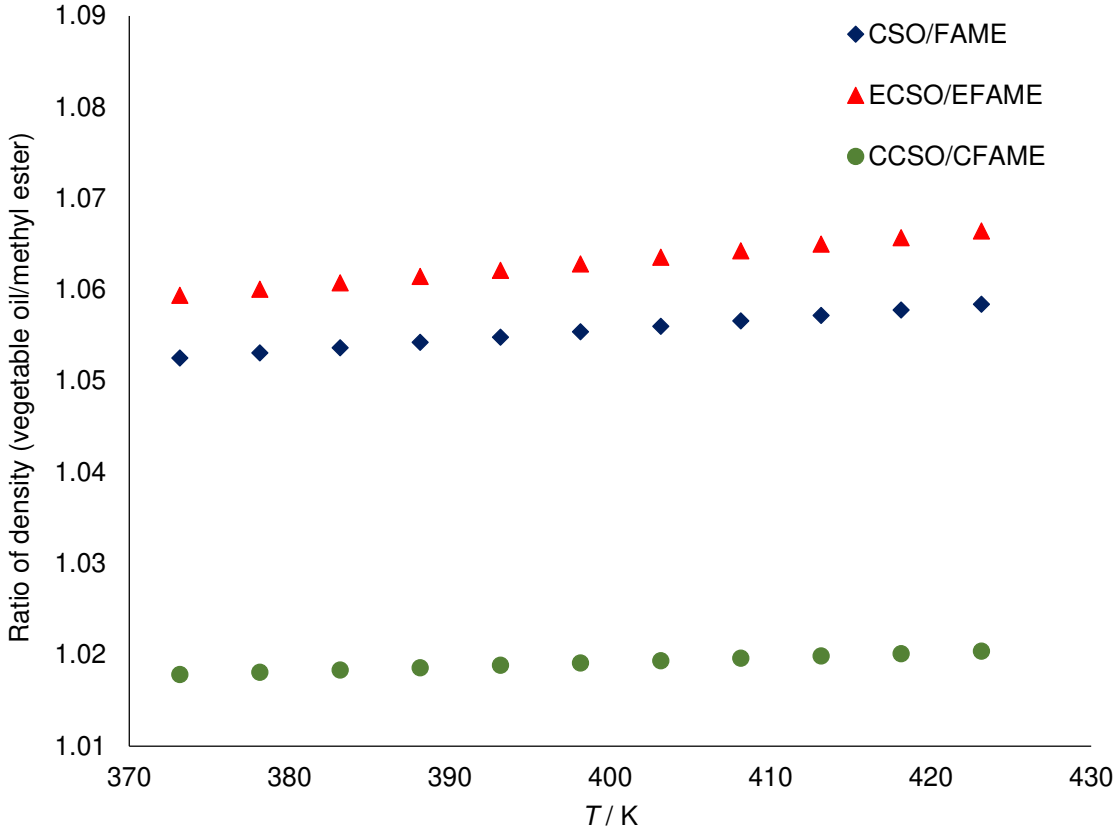

Figure 3. Ratio of $\frac{\rho_{CSO}}{\rho_{FAME}}$, $\frac{\rho_{ECSO}}{\rho_{EFAME}}$ and $\frac{\rho_{CCSO}}{\rho_{CFAME}}$ versus temperature

Figure 3 shows the evolution of density ratios: $\frac{\rho_{CSO}}{\rho_{FAME}}$, $\frac{\rho_{ECSO}}{\rho_{EFAME}}$ and $\frac{\rho_{CCSO}}{\rho_{CFAME}}$ versus temperature. One can notice that the ratios $\frac{\rho_{CSO}}{\rho_{FAME}}$ and $\frac{\rho_{ECSO}}{\rho_{EFAME}}$ are similar and equal to ca. 1.05, whereas the ratio $\frac{\rho_{CCSO}}{\rho_{CFAME}}$ is slightly smaller and equal to 1.02 in the temperature range 100-150°C. Thus, when the functional group is bigger, the difference of density between the vegetable oil and the methyl ester forms is lower.

Thus, the density for both systems is similar, and should not the main parameter explaining the difference of reactivity.

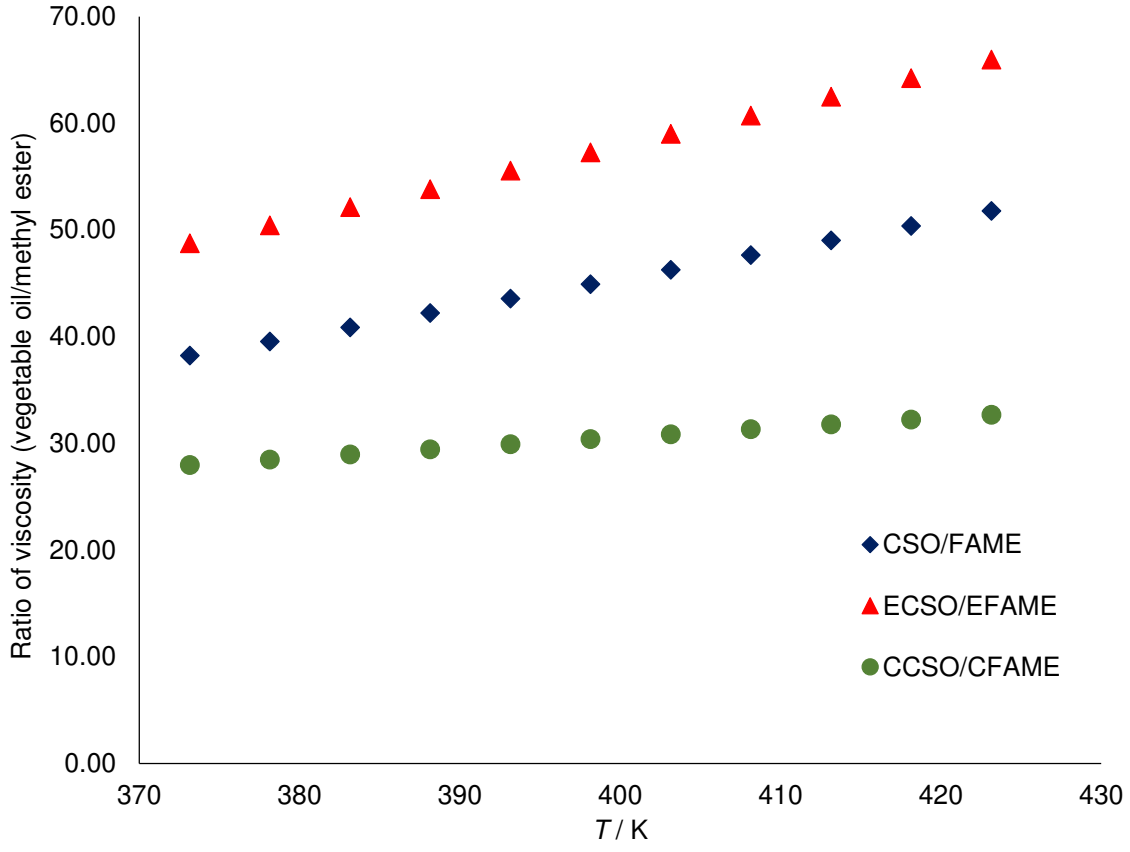

Figure 4. Ratio of $\frac{\mu_{CSO}}{\mu_{FAME}}$, $\frac{\mu_{ECSO}}{\mu_{EFAME}}$ and $\frac{\mu_{CCSO}}{\mu_{CFAME}}$ versus temperature

Figure 4 shows the evolution of viscosity ratios: $\frac{\mu_{CSO}}{\mu_{FAME}}$, $\frac{\mu_{ECSO}}{\mu_{EFAME}}$ and $\frac{\mu_{CCSO}}{\mu_{CFAME}}$ versus temperature. Unlike density behavior, the viscosity difference between vegetable oil and methyl ester derivatives is more pronounced. We clearly notice that viscosity of vegetable oil and its derivatives can be 20 to 40 times higher than the corresponding methyl ester and its derivatives.

This difference illustrates the benefit of using fatty acid methyl ester instead of vegetable oil from a mixing viewpoint.

In the case of mixture, the following correlations were used to determine the viscosity and density:[36]

$$\rho_{mixture} = w_{FAME} \times \rho_{FAME} + w_{EFAME} \times \rho_{EFAME} + w_{CFAME} \times \rho_{CFAME} \quad (2)$$

$$\ln \mu_{mixture} = w_{FAME} \times \ln \mu_{FAME} + w_{EFAME} \times \ln \mu_{EFAME} + w_{CFAME} \times \ln \mu_{CFAME} \quad (3)$$

where, w_i is the weight percentage of a compound *i* in mass fraction, wt %.

3.2. Mass transfer comparison

As described in the previous article of our group,[36,39] this stage is designed to measure the solubility of CO_2 and the kinetics of absorption in the reaction mixture. For that, two mass transfer parameters should be evaluated with the variation of functional groups, CO_2 pressure and temperature: Henry's constant and global mass transfer coefficient from the liquid side.

During the experiments, the pressure inside the reactor was maintained constant by using a pressure regulator, and the decrease of pressure inside the reservoir was monitored (Figure 2). The Whitman model was used to describe the mass transfer phenomenon.[42] Experiments were performed in the absence of catalyst to avoid any chemical reaction. The amount of CO_2

absorbed in the reaction mixture was assumed to be the same as the ones disappearing from the gas reservoir. Peng-Robinson equation of state was applied to determine the number of moles of CO_2 in the gas phase from the reservoir.

The mass balance of the components in the liquid phase can be expressed as

$$\frac{d[Ep]}{dt} = 0 \tag{4}$$

$$\frac{d[Carb]}{dt} = 0 \tag{5}$$

$$\frac{d[CO_2]_{Liq}}{dt} = \frac{k_L \cdot a}{V_{Liq}} \times \left(n^*_{CO_2,Liq} - n_{CO_2,Liq}\right) \tag{6}$$

where, [Ep] is the concentration of epoxidized group, $mol.L^{-1}$; [Carb] is the concentration of carbonated group, $mol.L^{-1}$; $[CO_2]_{Liq}$ is the concentration of CO_2 in the liquid phase, $mol.L^{-1}$; V_{Liq} is the volume of the liquid phase, m^3 and a is mass transfer ratio of the gas-liquid surface area to the volume of the liquid phase, m^{-1}. The term $n^*_{CO_2,Liq}$ is the equilibrium mole of CO_2 between the gas-liquid phase, mol, and $n_{CO_2,Liq}$ is the mole of CO_2 in the liquid phase at time t, mol.

Here, Eq.6 can be modified as

$$\frac{dn_{CO_2,Liq}}{dt} = k_L \cdot a \times \left(n^*_{CO_2,Liq} - n_{CO_2,Liq}\right) \tag{7}$$

where, $k_L.a$ is the gas-liquid volumetric mass transfer coefficient, s^{-1}.

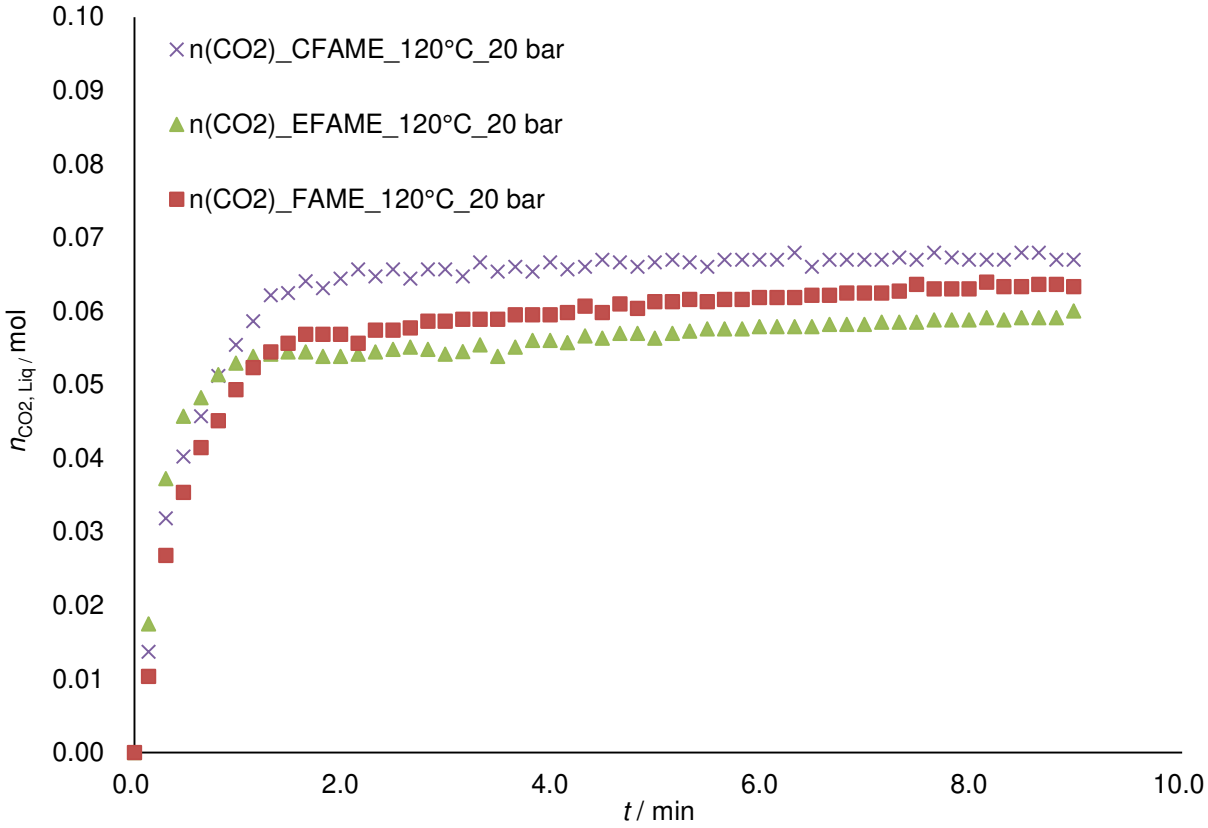

Figure 5. Effect of the composition on the kinetics of CO_2 absorption in the EFAME solution at 20 bar, 120 °C and rotating speed of 500 rpm

Figure 5 reveals that the kinetics of CO_2 absorption in the three solutions of different compounds are similar. The fitting of the model to these experimental data can be found in supporting information (Figures S7-S9). Nevertheless, the equilibrium is more sensitive to the chemical composition of the solution. Based on our previous research,[36,39] it was noticed that the kinetics of CO_2 absorption and the solubility of CO_2 in CSO, ECSO or CCSO were more pronounced. Figures S3-S6 show the influences of pressure and temperature on the kinetics of CO_2 absorption in the FAME, EFAME and CFAME solutions.

Henry's constant was used to describe the relationship between the solubility of CO_2 in the liquid phase and the pressure of CO_2 in the gas phase (Eq. 8).

$$[CO_2]^*_{Liq} = He \times P_{CO_2} \quad (8)$$

where, *He* is the Henry's constant for FAME, EFAME or CFAME. P_{CO_2} is the pressure of CO_2 in the gas phase.

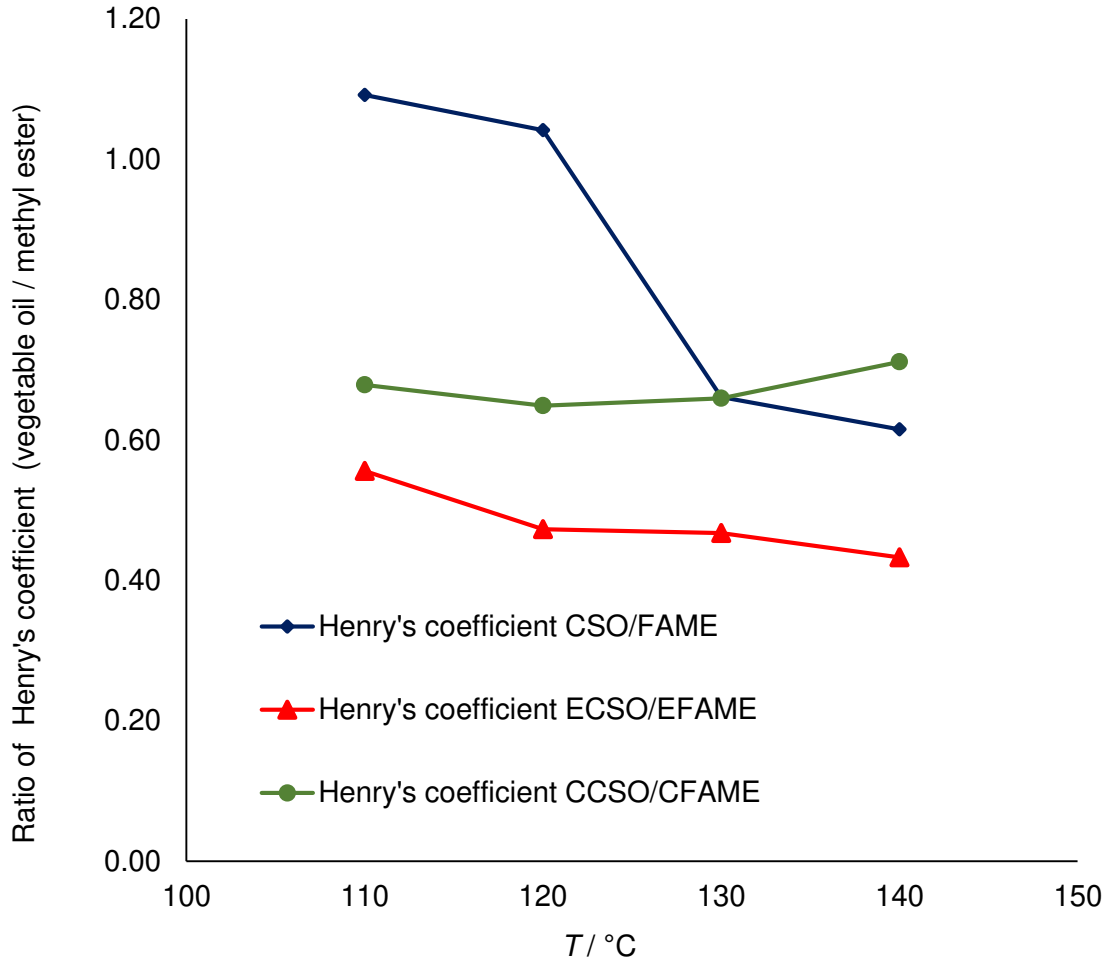

Figure 6. Ratio of $\frac{He_{CSO}}{He_{FAME}}$, $\frac{He_{ECSO}}{He_{EFAME}}$ and $\frac{He_{CCSO}}{He_{CFAME}}$ versus temperature.

Figure 6 shows the evolution of Henry's constant ratios: $\frac{He_{CSO}}{He_{FAME}}$, $\frac{He_{ECSO}}{He_{EFAME}}$ and $\frac{He_{CCSO}}{He_{CFAME}}$ versus temperature. Standard deviation for the value of Henry's constant was found to be

0.0014 mol.L^{-1}.bar^{-1}. The evolution of the Henry's constants with temperature is shown in Figure S14. These figures show that Henry's constants are different for a FAME and for a vegetable oil solution.

It indicates that the solubility of CO_2 follows the order of CFAME>EFAME>FAME when the temperature is higher than 120 °C. However, as shown in Figure S14, the solubility of CO_2 in the CFAME solution is lower than EFAME within the temperature of 110-120 °C. For CSO and its derivatives, it was observed that solubility of carbon dioxide increases in the following order CCSO>CSO≥ECSO when temperature is higher than 130 °C, but when temperature is within the range 110-120 °C the solubility is higher in CSO than CCSO or ECSO solution.

A van't Hoff law was used to describe the evolution of the Henry's constant with the temperature (Eq. 9).

$$\frac{He\ (T)}{He\ (T_{ref})} = \exp\left(\frac{-\Delta H_{sol,i}}{R} \times \left(\frac{1}{T} - \frac{1}{T_{ref}}\right)\right) \quad (9)$$

where, $\Delta H_{sol,i}$ is the dissolution enthalpy of CO_2 in the solution *i*. T_{ref} is the reference temperature. In the mass transfer study, 383.15K was used as the reference temperature in Eq. 9.

Based on the van't Hoff curve shown in Figure S15, it shows that the dissolution of CO_2 in FAME, EFAME and CFAME is an exothermic phenomenon: $\Delta H_{sol,FAME} = -11.83\ kJ.mol^{-1}$, $\Delta H_{sol,EFAME} = -17.31\ kJ.mol^{-1}$ and $\Delta H_{sol,CFAME} = -11.85\ kJ.mol^{-1}$. The enthalpies of dissolution of CO_2 in fatty methyl ester and its epoxidized derivatives are lower , in absolute value, compared to cottonseed oil ($\Delta H_{sol,CSO} = -40.41\ kJ.mol^{-1}$) and its epoxidized ($\Delta H_{sol,ECSO} = -29.03\ kJ.mol^{-1}$), respectively. However, the enthalpy of dissolution in

carbonated fatty acid methyl ester is similar to the one for carbonated cottonseed oil ($\Delta H_{sol,CCSO} = -11.52\,kJ.mol^{-1}$) derivative. Thus, the absorbed CO_2 has stronger interaction with CSO or ECSO systems than with the other ones. One explanation could be the steric conformation. In the case of CSO or ECSO, the functional groups are closer to each other, hence the absorbed CO_2 could higher number of interaction. In the case of FAME-derivatives and CCSO, the functional groups are distant.

From a thermodynamic viewpoint, solubility of CO_2 in FAME-derivatives is higher than CSO-derivatives, which is a benefit for the kinetics of carbonation.

As described in the previous work of our group,[36] the global mass transfer coefficient depends on temperature, dynamic viscosity (μ_{Liq}) and density (ρ_{Liq}) (Eq. 10).

$$k_L \cdot a = (k_L \cdot a)' \times \left(\frac{T_{Liq}}{\mu_{Liq}}\right)^{0.5} \times \left(\frac{\theta_{Liq}}{\mu_{Liq}}\right)^{0.25} \quad (10)$$

To take into account the chemical composition and temperature, a modified mass transfer coefficient ($k_L.a$)' was proposed as (Eq. 11):

$$(k_L \cdot a)' = \frac{2}{\sqrt{\pi}} \times \sqrt{\frac{7.4\times10^{-8} \times (\theta \times M_{Liq})}{V_{CO_2}^{0.6}}} \times (\varepsilon)^{0.25} \quad (11)$$

where, ρ_{Liq} is the density and μ_{Liq} is viscosity of the liquid phase; M_{Liq} is the molar mass of the liquid phase; V_{CO2} is the molar volume of the gas phase; θ is the association factor and ξ is the energy dissipation rate per unit mass.

To estimate ($k_L.a$)', the number of moles of CO_2 absorbed in the liquid phase was used as observable. The ordinary differential equation (Eq. 6) was solved out by using the solver ODESSA. The objective function ω (Eq. 12) was minimized by using simplex and Levenberg-Marquardt algorithms.

$$\omega = \sum \left(n_{CO_2,Liq} - \hat{n}_{CO_2,Liq} \right)^2 \quad (12)$$

where, $n_{CO_2,Liq}$ is the number of moles of CO_2 absorbed in the liquid phase obtained experimentally and $\hat{n}_{CO_2,Liq}$ is the ones obtained by simulation.

Figures 7-9 show some example of data fitting. One can notice that the model fits correctly the experimental data. The coefficient of determination was found to be 92% showing the good reliability of the model. Figures S4-S6 show the parity plot for the number of moles of absorbed CO_2 in the case of absorption for FAME-derivatives. From these Figures, one can notice that the developed model is reliable.

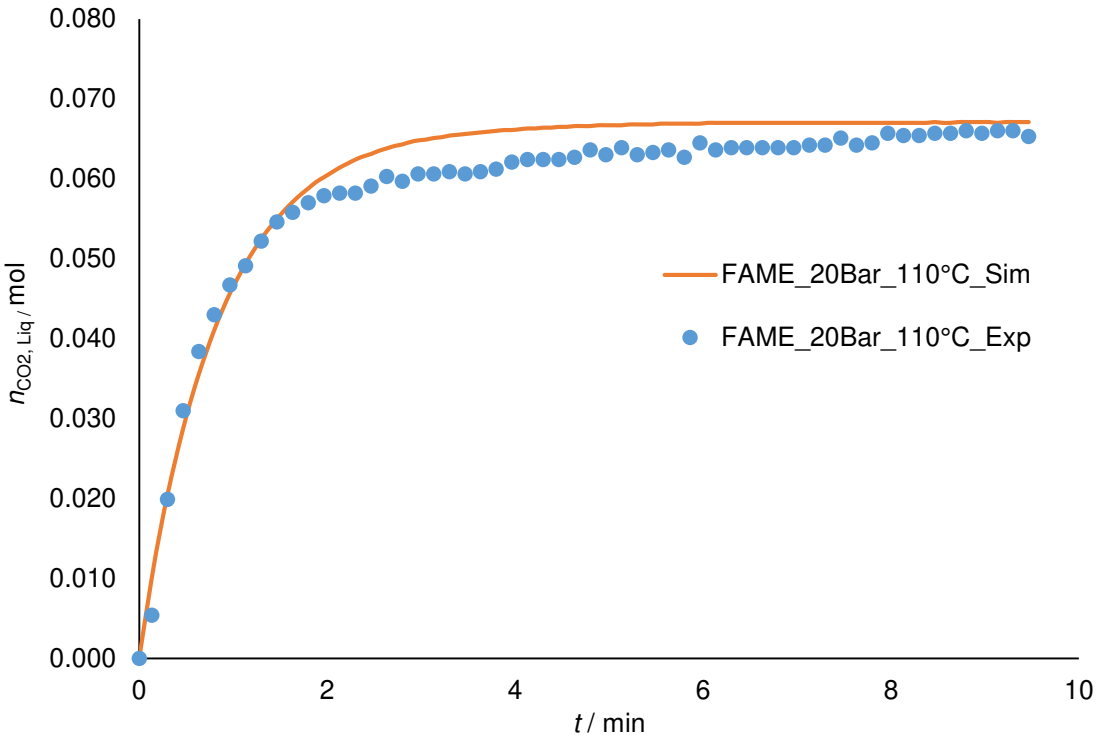

Figure 7. Fitting of the model to the experimental observation Run 9

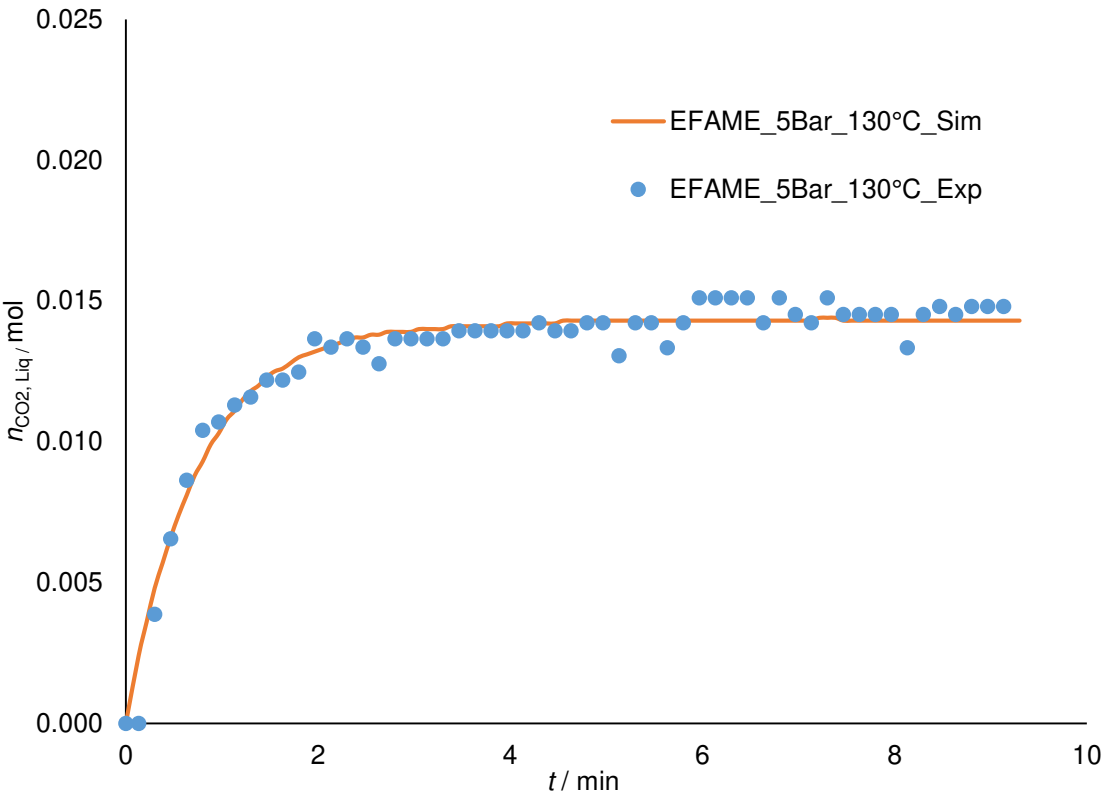

Figure 8. Fitting of the model to the experimental observation for Run 19

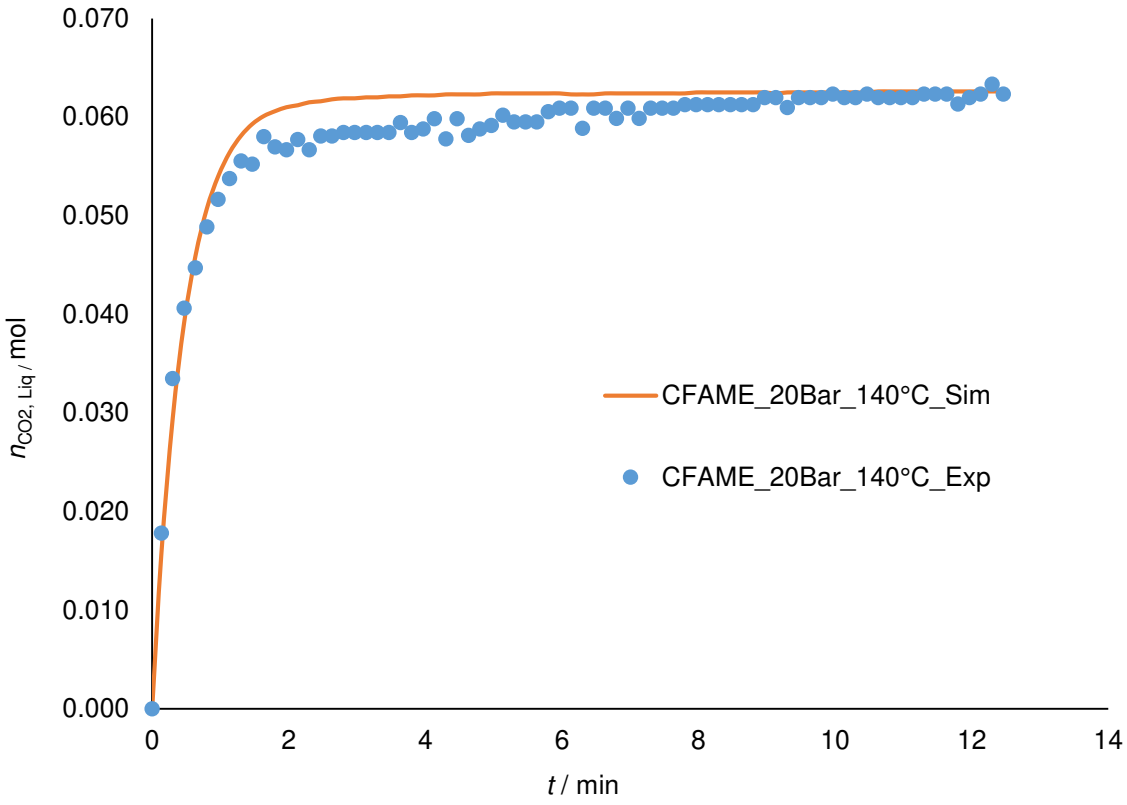

Figure 9. Fitting of the model to the experimental observation Run 44

The estimated values and their standard errors are shown in Table 2. For the sake of comparison, the data for CSO, CCSO and ECSO were included in Table 2.

Table 2. Estimated and statistical data for modified mass transfer coefficients

	Unit	Estimated value ($\times 10^{-6}$)	Standard error ($\times 10^{-8}$)	Standard error/ %
$(k_L \cdot a)'_{CFAME}$	$\left(\frac{K}{Pa \cdot s}\right)^{-0.5} \cdot \left(\frac{kg \cdot m^{-3}}{Pa \cdot s}\right)^{-0.25} s^{-1}$	2.59	8.3	3.2
$(k_L \cdot a)'_{EFAME}$	$\left(\frac{K}{Pa \cdot s}\right)^{-0.5} \cdot \left(\frac{kg \cdot m^{-3}}{Pa \cdot s}\right)^{-0.25} s^{-1}$	1.11	3.0	2.7
$(k_L \cdot a)'_{FAME}$	$\left(\frac{K}{Pa \cdot s}\right)^{-0.5} \cdot \left(\frac{kg \cdot m^{-3}}{Pa \cdot s}\right)^{-0.25} s^{-1}$	1.14	4.3	3.8
Modified Data from Cai et al. 2017				
$(k_L \cdot a)'_{CCSO}$	$\left(\frac{K}{Pa \cdot s}\right)^{-0.5} \cdot \left(\frac{kg \cdot m^{-3}}{Pa \cdot s}\right)^{-0.25} s^{-1}$	3.03	4.78	1.6
$(k_L \cdot a)'_{ECSO}$	$\left(\frac{K}{Pa \cdot s}\right)^{-0.5} \cdot \left(\frac{kg \cdot m^{-3}}{Pa \cdot s}\right)^{-0.25} s^{-1}$	12.3	23.0	1.9
$(k_L \cdot a)'_{CSO}$	$\left(\frac{K}{Pa \cdot s}\right)^{-0.5} \cdot \left(\frac{kg \cdot m^{-3}}{Pa \cdot s}\right)^{-0.25} s^{-1}$	25.7	42.2	1.6

From Table 2, one can see that the standard errors are low. The modified mass transfer coefficients are almost the same for CFAME and CCSO, but the ones of EFAME and FAME are ca. 100 times lower than ECSO and CSO.

To recap, solubility of CO_2 in methyl ester and its derivatives is higher than for CSO and its derivatives. The modified mass transfer coefficients $(k_L.a)'$ for methyl ester and epoxidized derivatives are lower than for CSO and ECSO.

Similarly to the previous study, in the case of mixture, the constants $(k_L.a)'$ and the Henry's constant were estimated as:[36]

$$\left(k_L \cdot a\right)'_{\text{mixture}} = w_{\text{FAME}} \times \left(k_L \cdot a\right)'_{\text{FAME}} + w_{\text{EFAME}} \times \left(k_L \cdot a\right)'_{\text{EFAME}} + w_{\text{CFAME}} \times \left(k_L \cdot a\right)'_{\text{CFAME}} \quad (13)$$

$$He_{\text{mixture}}\left(T\right) = x_{\text{FAME}} \times He_{\text{FAME}}\left(T\right) + x_{\text{EFAME}} \times He_{\text{EFAME}}\left(T\right) + x_{\text{CFAME}} \times He_{\text{CFAME}}\left(T\right) \quad (14)$$

where, w_i is the weight fraction of the compound *i*, wt %; *x* is the molar fraction of the functional group (double bond, epoxide group, carbonated group), %.

3.3. Kinetics comparison

The kinetic rate equation of carbonation reaction for the EFAME was firstly proposed on the basis of kinetic model for cottonseed oil, which is expressed as [36,43]

$$R_{\text{carbonation}} = \frac{k_{\text{carbonation}} \times \left[CO_2\right]_{\text{Liq}} \times \left[TBABr\right]^n \times \left(\left[Ep\right] + \gamma \times \left[Carb\right]\right)}{\alpha + \left[CO_2\right]_{\text{Liq}}} \quad (15)$$

where, $R_{\text{carbonation}}$ is the carbonation reaction rate, $mol.L^{-1}.s^{-1}$; $k_{\text{carbonation}}$ is the rate constant, $L^2.mol^{-2}.s^{-1}$; [TBABr] is the concentration of the catalyst TBABr, $mol.L^{-1}$; [Carb] is the concentration of carbonated group, $mol.L^{-1}$; n is the reaction order with respect to the catalyst; α and γ are the terms associated with the reaction constant. The same value of *n*, α and γ from the kinetic model for the carbonation of ECSO was used for the carbonation of EFAME, because the reaction mechanism should be the same (Table 3).

We have estimated the carbonation reaction rate constant $k_{\text{carbonation}}$ and the activation energy $Ea_{\text{carbonation}}$ for both systems.

Mass balance for the different species lead to the following ODEs:

$$\frac{d[Ep]}{dt} = -R_{\text{carbonation}} \quad (16)$$

$$\frac{d[Carb]}{dt} = +R_{\text{carbonation}} \quad (17)$$

$$\frac{d[CO_2]_{Liq}}{dt} = -R_{carbonation} + N_{CO_2} \times a \quad (18)$$

Where, Nco_2 is the interfacial component flux expressed by the Fick's law. The term $N_{CO_2} \times a$ represents for the gas-liquid transfer of CO_2 and it is expressed as follows:

$$N_{CO_2} \times a = k_L \cdot a \times \left([CO_2]^*_{Liq} - [CO_2]_{Liq}\right) \quad (19)$$

$$a = \frac{A}{V_{Liq}} \quad (20)$$

where, A is the gas-liquid surface area; V_{Liq} is the volume of the liquid phase.

The software MODEST was used to model the reaction kinetics and to solve out the ODEs system by using the ODESSA solver based on the backward difference methods.[44]

The concentration of epoxidized group was selected as the observable. The objective function ω was

$$\omega = \sum_i \left(C_i - \hat{C}_i\right)^2 \quad (21)$$

where, C_i represents the experimental obversable; $\hat{C}_i$ is the predicted value.

The objective function ω was minimized by using a Simplex and Levenberg-Marquardt algorithms. And, the explanation coefficient R^2 is defined as

$$R^2 = 1 - \frac{\left(C_i - \hat{C}_i\right)^2}{\left(C_i - \bar{C}_i\right)^2} \quad (22)$$

where, $\bar{C}_i$ stands for the average value.

Figures 10-11 show comparisons between the carbonation kinetic model fitting of ECSO and EFAME. One can notice that the kinetic model fits the experimental data. Both of the explanation coefficients for the kinetic of carbonation were found to be over 95%. Figures S16 and S17 show the parity plots for the concentration of epoxide groups in the case of the

carbonation of EFAME and ECSO. From these figures, one can notice that the kinetic models are reliable. The slight deviation of the model to the experimental data might due to the fact that quasi-equilibrium hypothesis was applied to the intermediate produced between the interaction of TBABr and the carbonated group. This reaction could be slower.

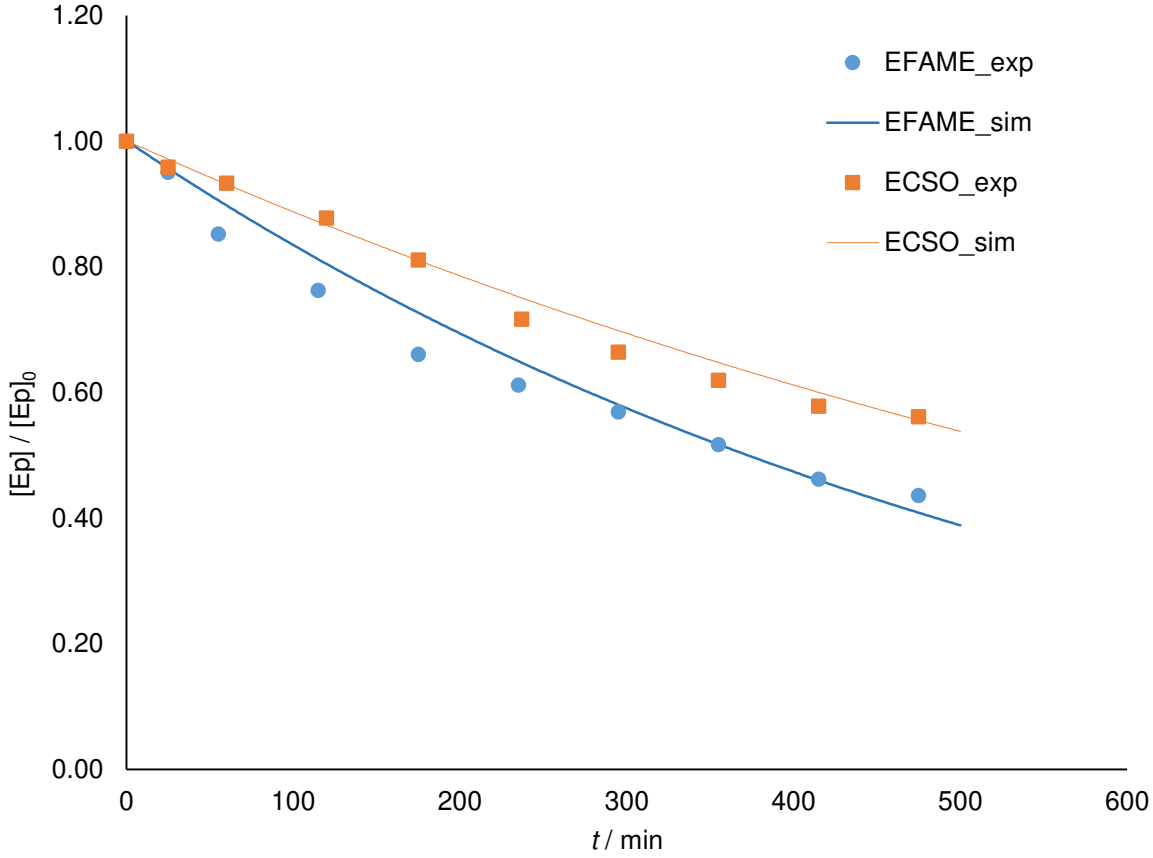

Figure 10. Fit of the model to the experiment data of $[Ep]/[EP]_0$ for Runs 53 and 61

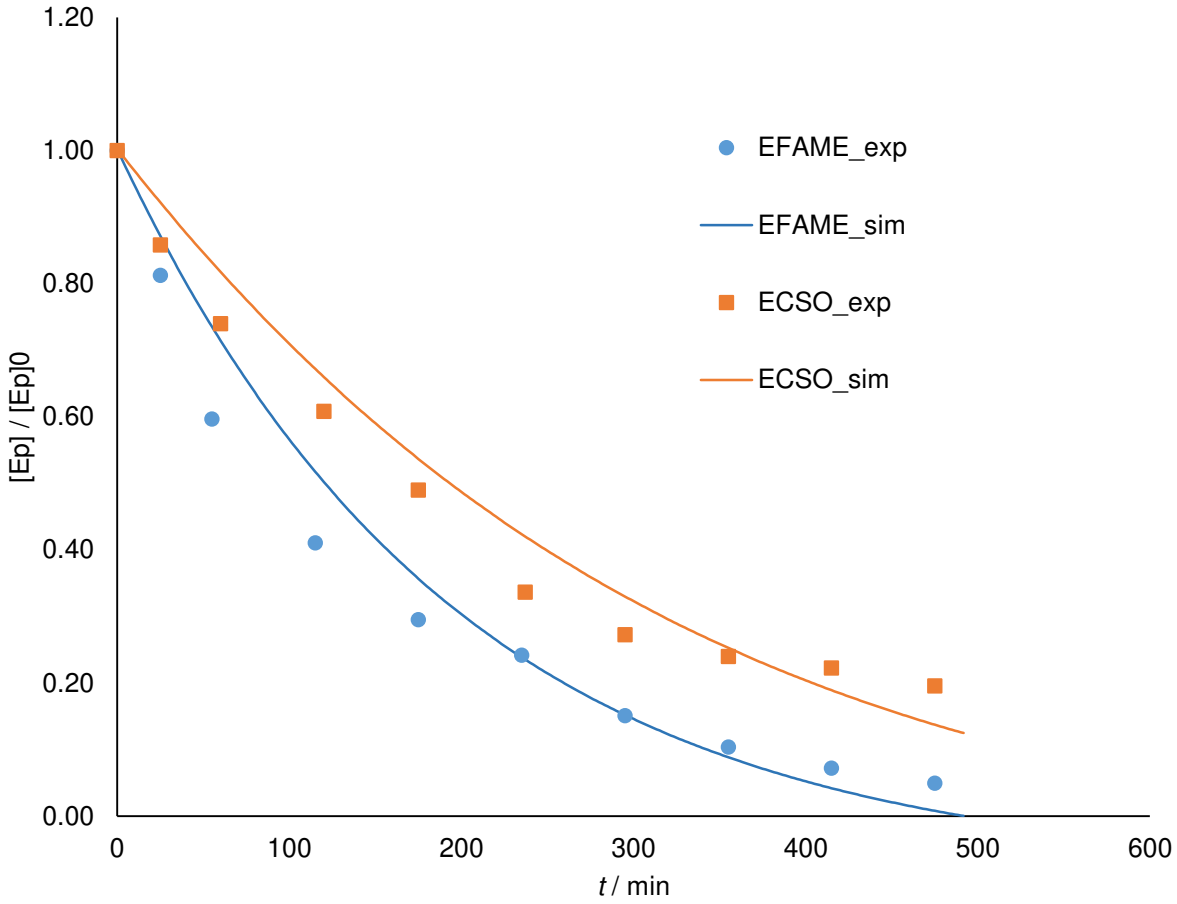

Figure 11. Fit of the model to the experiment data of $[Ep]/[EP]_0$ for Runs 55 and 65

Table 3. Estimated and statistical data at $T_{ref} = 403.15$ K for the carbonation of EFAME and ECSO

	Estimated	Standard error	Standard error %
$(k_{carbonation})_{EFAME}$ [$L^2.mol^{-2}.s^{-1}$]	2.57×10^{-4}	5.15×10^{-6}	2
$(Ea_{carbonation})_{EFAME}$ [$J.mol^{-1}$]	47200	2580	5.5
$(k_{carbonation})_{ECSO}$ [$L^2.mol^{-2}.s^{-1}$]	2.07×10^{-4}	3.35×10^{-5}	16.2
$(Ea_{carbonation})_{ECSO}$ [$J.mol^{-1}$]	50700	2930	5.8
n	0.584	0.0518	8.9
α [s^{-2}]	0.318	0.0924	29

γ [mol.L^{-1}]	0.078	0.0502	64.3

Table 3 shows the estimated kinetic data for the carbonation of EFAME. One can notice that the kinetics of carbonation of EFAME and ECSO are in the same order of magnitude.

Figure 12 shows the variation of reaction rate constant ratio of the carbonation of EFAME to ECSO at different reaction temperature.

One can notice from Figure 12 that there is a linear relationship between the ratio of $\frac{(k_{carbonation})_{ECSO}}{(k_{carbonation})_{EFAME}}$ and temperature. This linearity is due to similar values of kinetic constants.

One can notice that at low temperature, the rate of carbonation of EFAME is ca. 1.4 times higher than the rate of ECSO, while this difference is lower when temperature increases.

Thus, it suggests that it is possible to find a way to predict the reaction kinetics of vegetable oil if the reaction kinetics of its fatty acid methyl ester forms is known.

For both modeling systems, we have taken into account the evolution of density, viscosity, mass transfer coefficients and Henry's constants with temperature to estimate the kinetic constants. The difference of reactivity can be explained by steric hindrance which is more pronounced for vegetable oil derivatives. The reactivity centers, i.e., epoxide group of epoxidized FAME is more accessible than the ones of epoxidized vegetable oils.

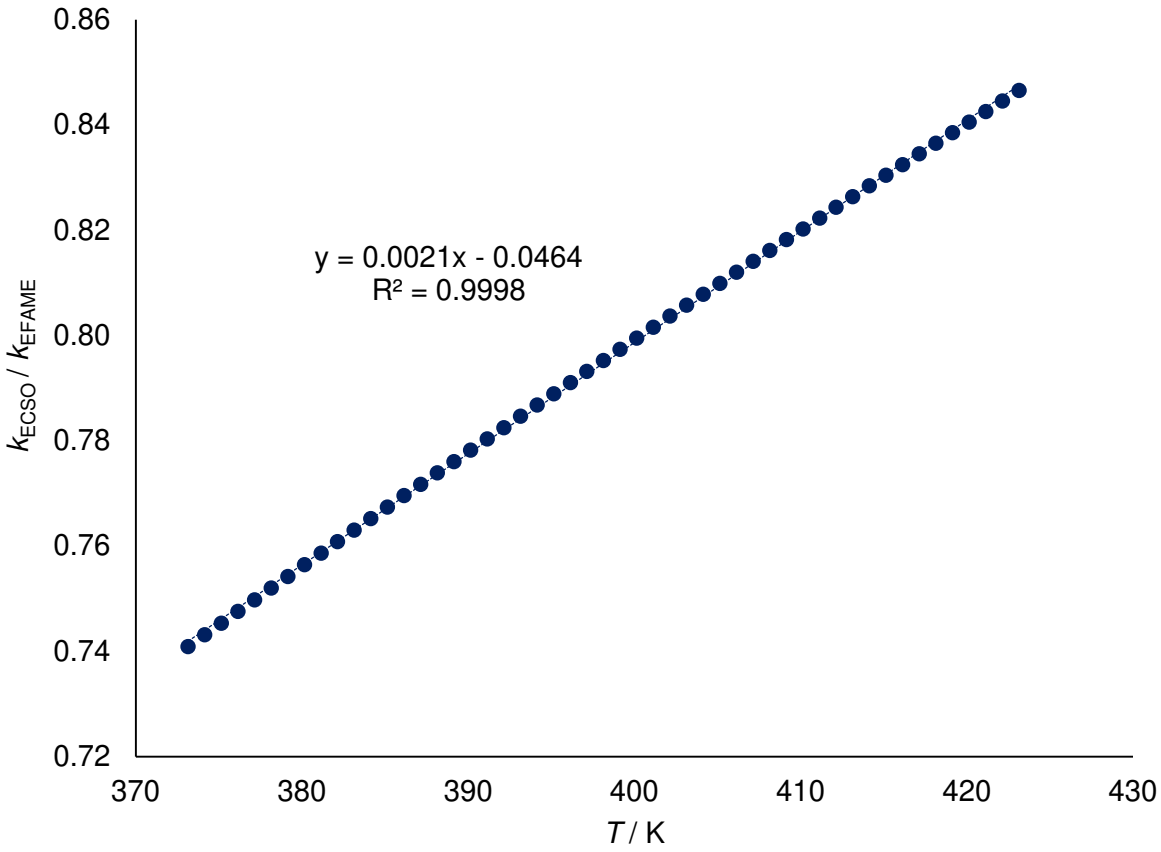

Figure 12. The variation of $\frac{(k_{\text{carbonation}})_{\text{ECSO}}}{(k_{\text{carbonation}})_{\text{EFAME}}}$ with different reaction temperature.

Conclusion

In this structure-reactivity paper, a comparison between the intrinsic carbonation kinetics of epoxidized cottonseed oil and the corresponding fatty acid methyl ester was performed by using homogeneous catalyst. Indeed, several studies proposed to transesterify vegetable oils, but none of them have proposed such comparison.

To perform such study, it is necessary to determine the Henry's constants and mass transfer coefficients. Because the global mass transfer coefficient depends on density and viscosity. Hence, these physicochemical properties were measured. We have found that density for both systems were similar. Nevertheless, the difference of viscosity is important, for instance, at 140 °C, we have observed that $\frac{\mu_{CSO}}{\mu_{FAME}} \approx 50$, $\frac{\mu_{ECSO}}{\mu_{EFAME}} \approx 40$ and $\frac{\mu_{CCSO}}{\mu_{CFAME}} \approx 20$.

The solubility of CO_2 was found to be higher in FAME-derivatives than in CSO-derivatives. Based on that, we have demonstrated that the carbonation rate constant of EFAME is higher than ECSO in the temperature range 100-150 °C. Furthermore, there exists a linear relationship between the reaction rate constant ratios of the carbonation of ECSO and EFAME. It suggested that it is possible to find a way to predict the reaction kinetics of vegetable oil base on the reaction kinetics of fatty acid methyl ester forms.

A continuation of this work could be to study more vegetable oils to see if the ratio of $\frac{(k_{carbonation})_{EVOs}}{(k_{carbonation})_{EFAME}}$ is always similar.

Acknowledgements

This study has been done in the framework of Task 2: “Green process: 2nd generation of biomass” of AMED project. The authors thank AMED project. The AMED project has been funded with the support from the European Union with the European Regional Development Fund (ERDF) and from the Regional Council of Normandie. Authors thank the China Scholarship Council: Co-operation Program with the UTs and INSAs (France).

The authors thank Justine Groscol for her help during the mass transfer study. The authors wish to thank Professors Dionisios G Vlachos and Dmitry Yu. Murzin for the fruitful discussion on this topic.

NOTATION

DB	double bond group
Ep	epoxide group
Carb	carbonated group
Ea	activation energy [kJ.mol^{-1}]
ΔH_R	reaction enthalpy [J.mol^{-1}]
k_i	rate constant of reaction *i*
R_i	reaction rate of reaction *i* [mol.L^{-1}.s^{-1}]
R	gas constant [J.K^{-1}.mol^{-1}]
T	temperature [K, °C]
T_{ref}	reference temperature [K, °C]
t	reaction time [min]
P	Pressure [bar]
w	weight percent [wt %]
R^2	coefficient of explanation [%]
V_{Liq}	volume of liquid phase [L]
$s(\theta_{mean})$	standard deviation of the mean
C_i	experimental obversable
$\hat{C}_i$	predicted value
He	Henry's constant [mol.L^{-1}.bar^{-1}]
$\Delta H_{sol,i}$	dissolution enthalpy of in the solution of compound *i* [J.mol^{-1}]
$n_{CO_2,Liq}$	number of moles of CO_2 absorbed in the liquid phase by experiment[mol]

$\hat{n}_{CO_2,Liq}$	number of moles of CO_2 absorbed in the liquid phase by simulation [mol]
$k_L.a$	volumetric mass transfer coefficient [s^{-1}]
$(k_L.a)'$	modified volumetric mass transfer coefficient [$(K.Pa^{-1}.s^{-1})^{-0.5}$. $(kg.m^{-3}.Pa^{-1}.s^{-1})^{-0.25}.s^{-1}$]

Greek letters

ξ	energy dissipation rate per unit mass [$W.kg^{-1}$]
ρ	mass density [$kg.L^{-1}$]
μ	viscosity [Pa.s]
ω	objective function

Subscripts and superscripts

Ep	Epoxidation substrates
Carb	Carbonation substrates
VO	vegetable oil
Liq	Liquid phase
Exp	experimental data
Sim	simulation data
i	component i
ref	reference state
*	interface

Abbreviations

CSO	cottonseed oil
FAME	cottonseed oil fatty acid methyl ester
ECSO	epoxidized cottonseed oil
EFAME	epoxidized cottonseed oil fatty acid methyl ester

CCSO	carbonated cottonseed oil
CFAME	carbonated cottonseed oil fatty acid methyl ester
CO_2	carbon dioxide
TBABr	tetra-n-butylammonium bromide
TEAB	tetraethylammonium bromide
ODEs	ordinary differential equations

ASSOCIATED CONTENT

Supporting Information

Density and viscosity of cottonseed oil/derivatives and fatty acid methyl ester/derivatives; effects of CO_2 pressure on the kinetics of CO_2 absorption in the EFAME solution, and temperature on the kinetics of CO_2 absorption in the FAME, EFAME and CFAME solutions; evolutions of the solubility of CO_2 at different CO_2 pressure for FAME, EFAME and CFAME; Van't Hoff curve for Henry's constants, evolution of a' and b' for the density and Arrhenius data are provided.

Tables

Figure captions

References

(1) Alptekin, E.; Canakci, M. Optimization of Pretreatment Reaction for Methyl Ester Production from Chicken Fat. *Fuel* **2010**, *89* (12), 4035–4039. https://doi.org/10.1016/j.fuel.2010.04.031.

(2) Che Mat, S.; Idroas, M. Y.; Hamid, M. F.; Zainal, Z. A. Performance and Emissions of Straight Vegetable Oils and Its Blends as a Fuel in Diesel Engine: A Review. *Renew. Sustain. Energy Rev.* **2018**, *82*, 808–823. https://doi.org/10.1016/j.rser.2017.09.080.

(3) Goldstein, I. S. *Organic Chemicals From Biomass*; CRC Press, 2018.

(4) Mohanty, A. K.; Misra, M.; Drzal, L. T. Sustainable Bio-Composites from Renewable Resources: Opportunities and Challenges in the Green Materials World. *J. Polym. Environ.* **2002**, *10* (1–2), 19–26. https://doi.org/10.1023/A:1021013921916.

(5) Murawski, A.; Quirino, R. L. Vegetable Oils as a Chemical Platform. In *Polymer Gels: Perspectives and Applications*; Thakur, V. K., Thakur, M. K., Voicu, S. I., Eds.; Gels Horizons: From Science to Smart Materials; Springer Singapore: Singapore, 2018; pp 125–152. https://doi.org/10.1007/978-981-10-6080-9_6.

(6) Fukuda, H.; Kondo, A.; Noda, H. Biodiesel Fuel Production by Transesterification of Oils. *J. Biosci. Bioeng.* **2001**, *92* (5), 405–416. https://doi.org/10.1016/S1389-1723(01)80288-7.

(7) Körbitz, W. Biodiesel Production in Europe and North America, an Encouraging Prospect. *Renew. Energy* **1999**, *16* (1), 1078–1083. https://doi.org/10.1016/S0960-1481(98)00406-6.

(8) Leung, D. Y. C.; Wu, X.; Leung, M. K. H. A Review on Biodiesel Production Using Catalyzed Transesterification. *Appl. Energy* **2010**, *87* (4), 1083–1095. https://doi.org/10.1016/j.apenergy.2009.10.006.

(9) Santacesaria, E.; Vicente, G. M.; Di Serio, M.; Tesser, R. Main Technologies in Biodiesel Production: State of the Art and Future Challenges. *Catal. Today* **2012**, *195* (1), 2–13. https://doi.org/10.1016/j.cattod.2012.04.057.

(10) Di Serio, M.; Tesser, R.; Pengmei, L.; Santacesaria, E. Heterogeneous Catalysts for Biodiesel Production. *Energy Fuels* **2008**, *22* (1), 207–217. https://doi.org/10.1021/ef700250g.

(11) Silva, S. P.; Sales, D. C. S.; de Abreu, C. A. P.; Schuler, A. R. P.; de Abreu, C. A. M. Kinetics of the Biphasic Liquid–Liquid Transesterification of Vegetable Oils into Biodiesel. *React. Kinet. Mech. Catal.* **2018**, *123* (2), 529–542. https://doi.org/10.1007/s11144-017-1322-8.

(12) Andreo-Martínez, P.; García-Martínez, N.; Durán-del-Amor, M. del M.; Quesada-Medina, J. Advances on Kinetics and Thermodynamics of Non-Catalytic Supercritical Methanol Transesterification of Some Vegetable Oils to Biodiesel. *Energy Convers. Manag.* **2018**, *173*, 187–196. https://doi.org/10.1016/j.enconman.2018.07.069.

(13) Ullah, Z.; Khan, A. S.; Muhammad, N.; Ullah, R.; Alqahtani, A. S.; Shah, S. N.; Ghanem, O. B.; Bustam, M. A.; Man, Z. A Review on Ionic Liquids as Perspective Catalysts in Transesterification of Different Feedstock Oil into Biodiesel. *J. Mol. Liq.* **2018**, *266*, 673–686. https://doi.org/10.1016/j.molliq.2018.06.024.

(14) Ullah, Z.; Bustam, M. A.; Man, Z. Biodiesel Production from Waste Cooking Oil by Acidic Ionic Liquid as a Catalyst. *Renew. Energy* **2015**, *77*, 521–526. https://doi.org/10.1016/j.renene.2014.12.040.

(15) Marchetti, J. M.; Miguel, V. U.; Errazu, A. F. Possible Methods for Biodiesel Production. *Renew. Sustain. Energy Rev.* **2007**, *11* (6), 1300–1311. https://doi.org/10.1016/j.rser.2005.08.006.

(16) Demirbas, A. Relationships Derived from Physical Properties of Vegetable Oil and Biodiesel Fuels. *Fuel* **2008**, *87* (8), 1743–1748. https://doi.org/10.1016/j.fuel.2007.08.007.

(17) Demirbaş, A. Biodiesel from Vegetable Oils via Transesterification in Supercritical Methanol. *Energy Convers. Manag.* **2002**, *43* (17), 2349–2356. https://doi.org/10.1016/S0196-8904(01)00170-4.

(18) Rastogi, N. K.; Raghavarao, K. S. M. S.; Niranjan, K.; Knorr, D. Recent Developments in Osmotic Dehydration: Methods to Enhance Mass Transfer. *Trends Food Sci. Technol.* **2002**, *13* (2), 48–59. https://doi.org/10.1016/S0924-2244(02)00032-8.

(19) Abdullah, B. M.; Salimon, J. Epoxidation of Vegetable Oils and Fatty Acids: Catalysts, Methods and Advantages. *J. Appl. Sci.* **2010**, *10* (15), 1545–1553.

(20) Desroches, M.; Benyahya, S.; Besse, V.; Auvergne, R.; Boutevin, B.; Caillol, S. Synthesis of Bio-Based Building Blocks from Vegetable Oils: A Platform Chemicals Approach. *Lipid Technol.* **2014**, *26* (2), 35–38. https://doi.org/10.1002/lite.201400014.

(21) Fox, N. J.; Stachowiak, G. W. Vegetable Oil-Based Lubricants—A Review of Oxidation. *Tribol. Int.* **2007**, *40* (7), 1035–1046. https://doi.org/10.1016/j.triboint.2006.10.001.

(22) Carbonell-Verdu, A.; Garcia-Sanoguera, D.; Jordá-Vilaplana, A.; Sanchez-Nacher, L.; Balart, R. A New Biobased Plasticizer for Poly(Vinyl Chloride) Based on Epoxidized Cottonseed Oil. *J. Appl. Polym. Sci.* **2016**, *133* (27). https://doi.org/10.1002/app.43642.

(23) Chandrasekara, G.; Mahanama, M. K.; Edirisinghe, D. G.; Karunanayake, L. Epoxidized Vegetable Oils as Processing Aids and Activators in Carbon-Black Filled Natural Rubber Compounds. *J. Natl. Sci. Found. Sri Lanka* **2011**, *39* (3), 243–250.

(24) Saurabh, T.; Patnaik, M.; Bhagt, S.; Renge, V. Epoxidation of Vegetable Oils: A Review. *Int. J. Adv. Eng. Technol.* **2011**, *2*, 491–501.

(25) Hosney, H.; Nadiem, B.; Ashour, I.; Mustafa, I.; El- Shibiny, A. Epoxidized Vegetable Oil and Bio-Based Materials as PVC Plasticizer. *J. Appl. Polym. Sci.* **2018**, *135* (20), 46270. https://doi.org/10.1002/app.46270.

(26) Wisniak, J.; Cancino, A.; Vega, J. C. Epoxidation of Anchovy Oils. A Study of Variables. *IEC Prod. Res. Dev.* **1964**, *3* (4), 306–311. https://doi.org/10.1021/i360012a012.

(27) Campanella, A.; Fontanini, C.; Baltanás, M. A. High Yield Epoxidation of Fatty Acid Methyl Esters with Performic Acid Generated in Situ. *Chem. Eng. J.* **2008**, *144* (3), 466–475. https://doi.org/10.1016/j.cej.2008.07.016.

(28) Santacesaria, E.; Tesser, R.; Di Serio, M.; Turco, R.; Russo, V.; Verde, D. A Biphasic Model Describing Soybean Oil Epoxidation with H2O2 in a Fed-Batch Reactor. *Chem. Eng. J.* **2011**, *173* (1), 198–209. https://doi.org/10.1016/j.cej.2011.05.018.

(29) Goud, V. V.; Patwardhan, A. V.; Dinda, S.; Pradhan, N. C. Kinetics of Epoxidation of Jatropha Oil with Peroxyacetic and Peroxyformic Acid Catalysed by Acidic Ion

Exchange Resin. *Chem. Eng. Sci.* **2007**, *62* (15), 4065–4076. https://doi.org/10.1016/j.ces.2007.04.038.

(30) Zheng, J. L.; Wärnå, J.; Salmi, T.; Burel, F.; Taouk, B.; Leveneur, S. Kinetic Modeling Strategy for an Exothermic Multiphase Reactor System: Application to Vegetable Oils Epoxidation Using Prileschajew Method. *AIChE J.* **2016**, *62* (3), 726–741. https://doi.org/10.1002/aic.15037.

(31) Huang, Y. B.; Yao, M. Y.; Xin, P. P.; Zhou, M. chao; Yang, T.; Pan, H. Influence of Alkenyl Structures on the Epoxidation of Unsaturated Fatty Acid Methyl Esters and Vegetable Oils. *RSC Adv.* **2015**, *5* (91), 74783–74789. https://doi.org/10.1039/C5RA11035A.

(32) Omonov, T. S.; Kharraz, E.; Curtis, J. M. The Epoxidation of Canola Oil and Its Derivatives. *RSC Adv.* **2016**, *6* (95), 92874–92886. https://doi.org/10.1039/C6RA17732H.

(33) Cai, X.; Zheng, J. L.; Aguilera, A. F.; Vernières- Hassimi, L.; Tolvanen, P.; Salmi, T.; Leveneur, S. Influence of Ring-Opening Reactions on the Kinetics of Cottonseed Oil Epoxidation. *Int. J. Chem. Kinet.* **2018**, *50* (10), 726–741. https://doi.org/10.1002/kin.21208.

(34) Aguilera, A. F.; Tolvanen, P.; Heredia, S.; Muñoz, M. G.; Samson, T.; Oger, A.; Verove, A.; Eränen, K.; Leveneur, S.; Mikkola, J.-P.; et al. Epoxidation of Fatty Acids and Vegetable Oils Assisted by Microwaves Catalyzed by a Cation Exchange Resin. *Ind. Eng. Chem. Res.* **2018**, *57* (11), 3876–3886. https://doi.org/10.1021/acs.iecr.7b05293.

(35) Cai, X.; Ait Aissa, K.; Estel, L.; Leveneur, S. Investigation of the Physicochemical Properties for Vegetable Oils and Their Epoxidized and Carbonated Derivatives. *J. Chem. Eng. Data* **2018**, *63* (5), 1524–1533. https://doi.org/10.1021/acs.jced.7b01075.

(36) Cai, X.; Zheng, J. L.; Wärnå, J.; Salmi, T.; Taouk, B.; Leveneur, S. Influence of Gas-Liquid Mass Transfer on Kinetic Modeling: Carbonation of Epoxidized Vegetable Oils. *Chem. Eng. J.* **2017**, *313*, 1168–1183. https://doi.org/10.1016/j.cej.2016.11.012.

(37) Ait Aissa, K.; Zheng, J. L.; Estel, L.; Leveneur, S. Thermal Stability of Epoxidized and Carbonated Vegetable Oils. *Org. Process Res. Dev.* **2016**, *20* (5), 948–953. https://doi.org/10.1021/acs.oprd.6b00040.

(38) Pérez-Sena, W. Y.; Cai, X.; Kebir, N.; Vernières-Hassimi, L.; Serra, C.; Salmi, T.; Leveneur, S. Aminolysis of Cyclic-Carbonate Vegetable Oils as a Non-Isocyanate Route for the Synthesis of Polyurethane: A Kinetic and Thermal Study. *Chem. Eng. J.* **2018**, *346*, 271–280. https://doi.org/10.1016/j.cej.2018.04.028.

(39) Zheng, J. L.; Burel, F.; Salmi, T.; Taouk, B.; Leveneur, S. Carbonation of Vegetable Oils: Influence of Mass Transfer on Reaction Kinetics. *Ind. Eng. Chem. Res.* **2015**, *54* (43), 10935–10944. https://doi.org/10.1021/acs.iecr.5b02006.

(40) Maerker, G. Determination of Oxirane Content of Derivatives of Fats. *J. Am. Oil Chem. Soc.* **1965**, *42* (4), 329–332.

(41) Paquot, C. *Standard Methods for the Analysis of Oils, Fats and Derivatives*; Elsevier, 2013.

(42) Charpentier, J.-C. Mass-Transfer Rates in Gas-Liquid Absorbers and Reactors. In *Advances in Chemical Engineering*; Drew, T. B., Cokelet, G. R., Hoopes, J. W.,

Vermeulen, T., Eds.; Academic Press, 1981; Vol. 11, pp 1–133. https://doi.org/10.1016/S0065-2377(08)60025-3.

(43) Wilke, C. R.; Chang, P. Correlation of Diffusion Coefficients in Dilute Solutions. *AIChE J.* **1955**, *1* (2), 264–270.

(44) H. Haario. *MODEST-User's Guide*; Profmath Oy: Helsinki, 2001.

Supporting Information

Structure-reactivity: comparison between the carbonation of epoxidized vegetable oils and the corresponding epoxidized fatty acid methyl ester

Xiaoshuang Cai[a], *Manoelito Matos*[a], *Sébastien Leveneur*[a,b]*

[a] Normandie Univ, INSA Rouen, UNIROUEN, LSPC- Laboratoire de sécurité des procédés chimiques, EA4704, 76000 Rouen, France.

[b]Laboratory of Industrial Chemistry and Reaction Engineering, Process Chemistry Centre, Åbo Akademi University, Biskopsgatan 8, FI-20500 Åbo/Turku, Finland.

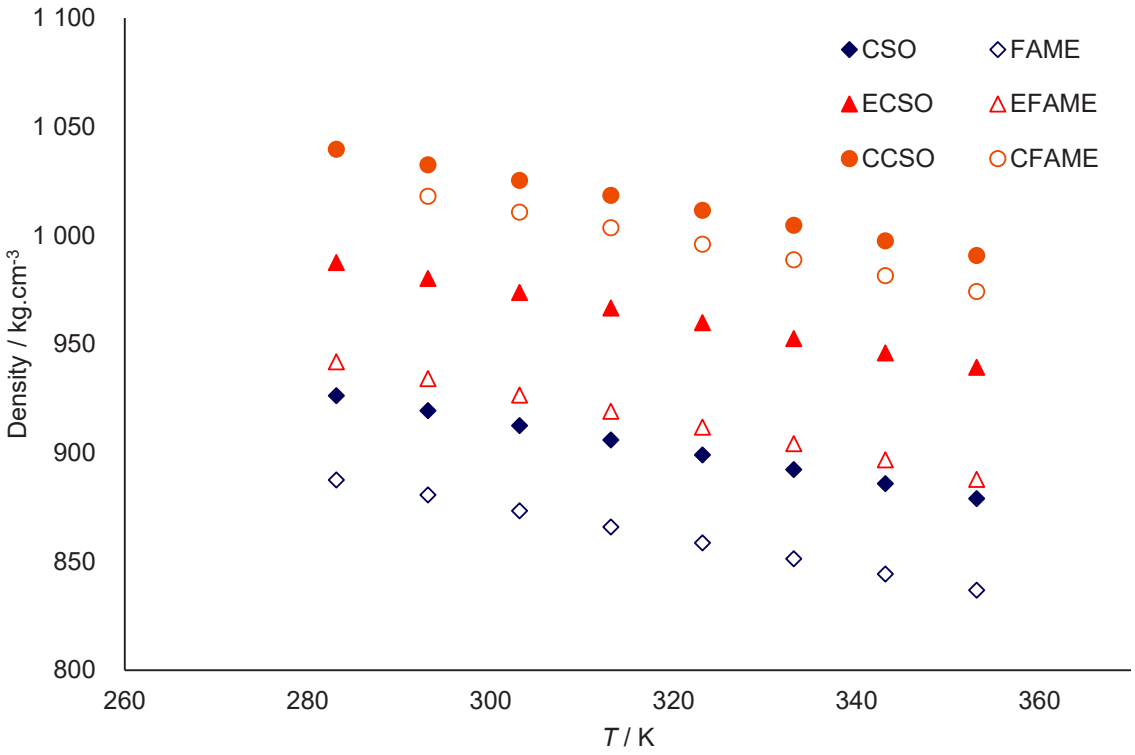

Figure S1. Density of cottonseed oil/derivatives and fatty acid methyl ester/derivatives

As shown in Figure S1, the density curves for CSO and FAME and their corresponding derivatives are parallels. As mentioned in our previous article [14], there is a linear relationship between density and temperature, which is expressed as

$$\rho = a' \times T + b' \quad (1)$$

where ρ is the density, kg.cm^{-3}; a' and b' are two constants; T is temperature, K.

Values of a' and b' for FAME and its derivatives are displayed in Table S1. The values of a' and b' for CSO and its derivatives can be found in the article of Cai et al. 2018 [14]. One can also notice that as functional groups are big, the density is higher, which resulting in the order of density as $\rho_{Carb} > \rho_{Ep} > \rho_{VO}$.

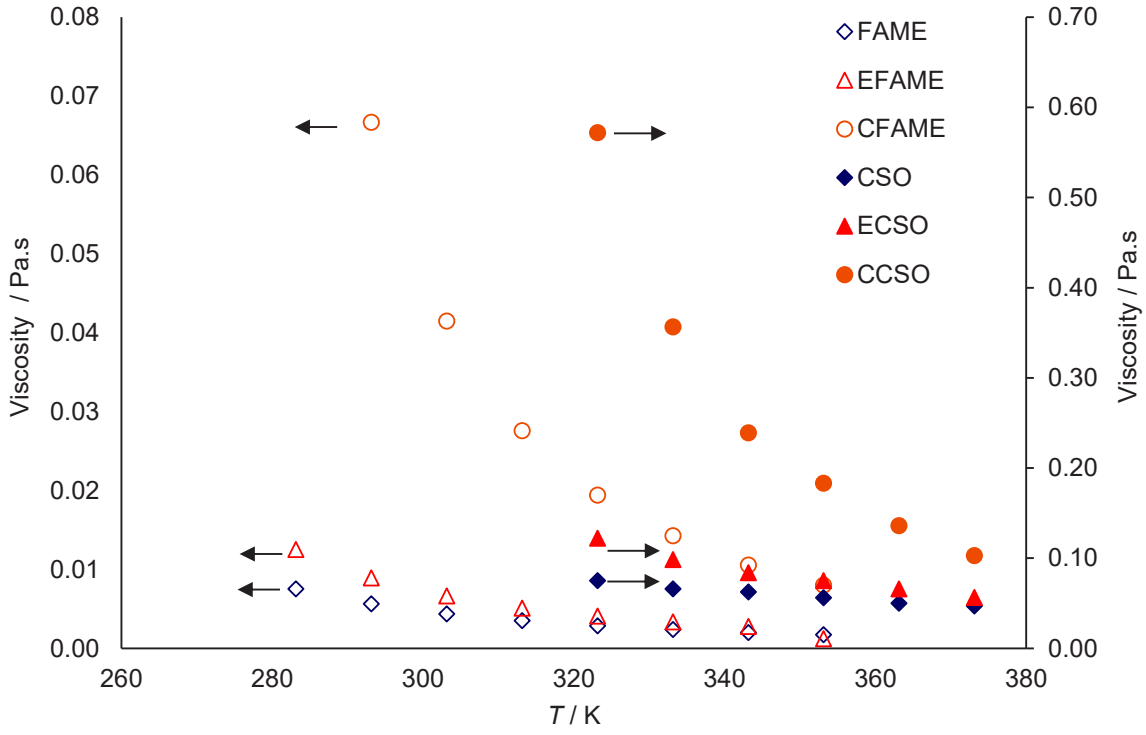

Figure S2. Viscosity of cottonseed oil/derivatives and fatty acid methyl ester/derivatives

As mentioned in the literature [14], cottonseed oil and its epoxidized and carbonated derivatives were found to be Newtonian fluids. In this study, we have also found that methyl ester and its

derivatives are Newtonian fluids. From Figure S2, one can see that viscosities evolve as: $\mu_{CSO} < \mu_{ECSO} < \mu_{CCSO}$ & $\mu_{FAME} < \mu_{EFAME} < \mu_{CFAME}$, and $\mu_{FAME} < \mu_{CSO}$, $\mu_{EFAME} < \mu_{ECSO}$ and $\mu_{CFAME} < \mu_{CCSO}$. This tendency confirms the fact that functional groups (double bond, epoxide group and carbonated group) have a strong influence on the viscosity value.

The correlation between viscosity and temperature can be expressed as follows:

$$\mu = A \times e^{-Ea/RT} \qquad (2)$$

where μ is the dynamic viscosity, Pa.s; A is the pre-exponential factor; Ea is the activation energy, J.mol^{-1}; R is the universal gas constant; T is temperature, K.

The Arrhenius constants for CSO, FAME, and its epoxidized and carbonated derivatives are displayed in Table S2.

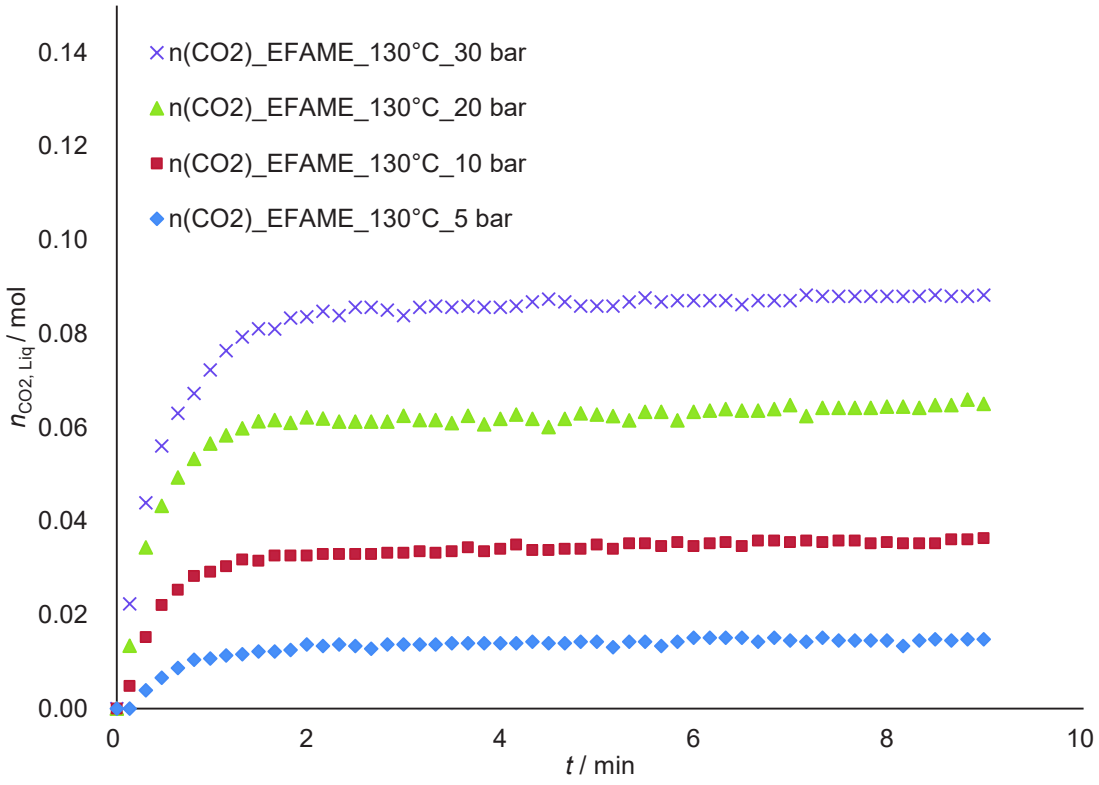

Figure S3. Effect of CO_2 pressure on the kinetics of CO_2 absorption in the EFAME solution at 130 °C and rotating speed of 500 rpm

Figure S3 shows the influence of CO_2 pressure on the kinetics of CO_2 absorption in the EFAME solution at 130 °C. It indicated that when the reaction pressure increases, the mass transfer of CO_2 goes faster, and the dissolution of CO_2 in the liquid phase becomes larger. This tendency is the same than for the absorption of CO_2 in ECSO.

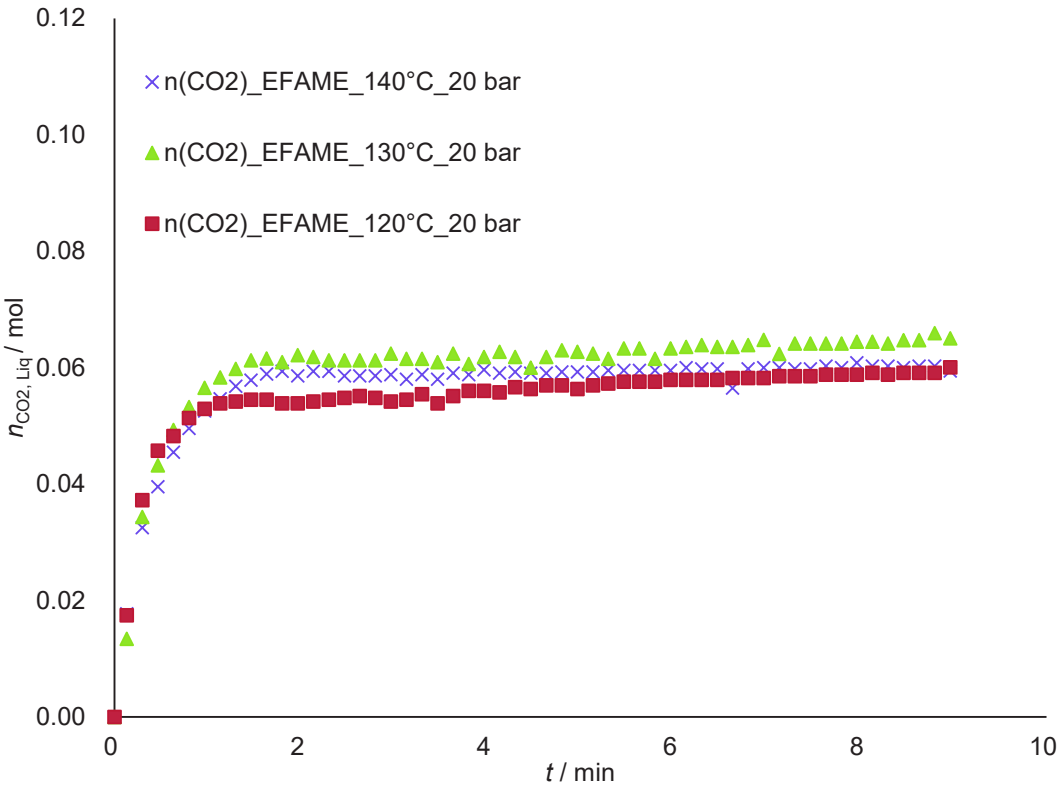

Figure S4. Effect of temperature on the kinetics of CO_2 absorption in the EFAME solution at 20 bar and rotating speed of 500 rpm

Figure S4 shows the influence of temperature on the kinetics of CO_2 absorption in the EFAME solution at 20 bar. It can be noticed that when the reaction temperature increases, the kinetics of CO_2 absorption does not change significantly. The dissolution of CO_2 in the liquid phase decreases when the temperature increases. The similar situation was noticed in Figures S5-S6 for adsorption of CO_2 in FAME and CFAME solution.

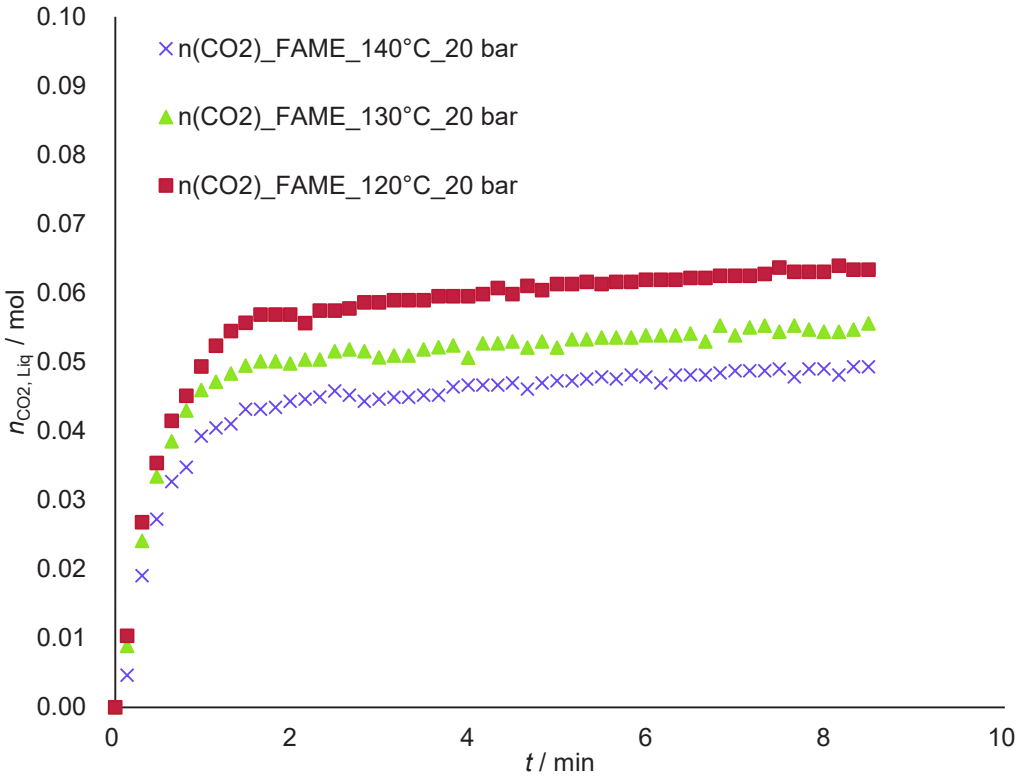

Figure S5. Effect of temperature on the kinetics of CO_2 absorption in the FAME solution at 20 bar and rotating speed of 500 rpm

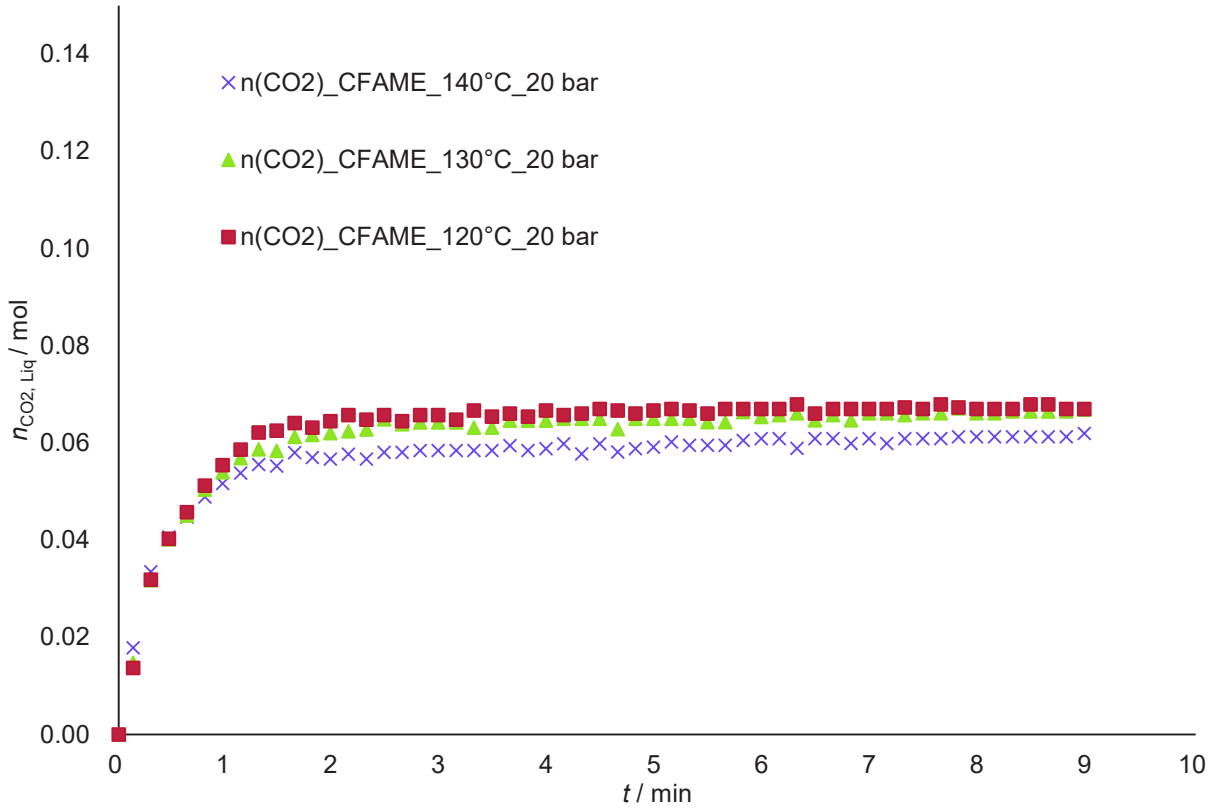

Figure S6. Effect of temperature on the kinetics of CO_2 absorption in the CFAME solution at 20 bar and rotating speed of 500 rpm

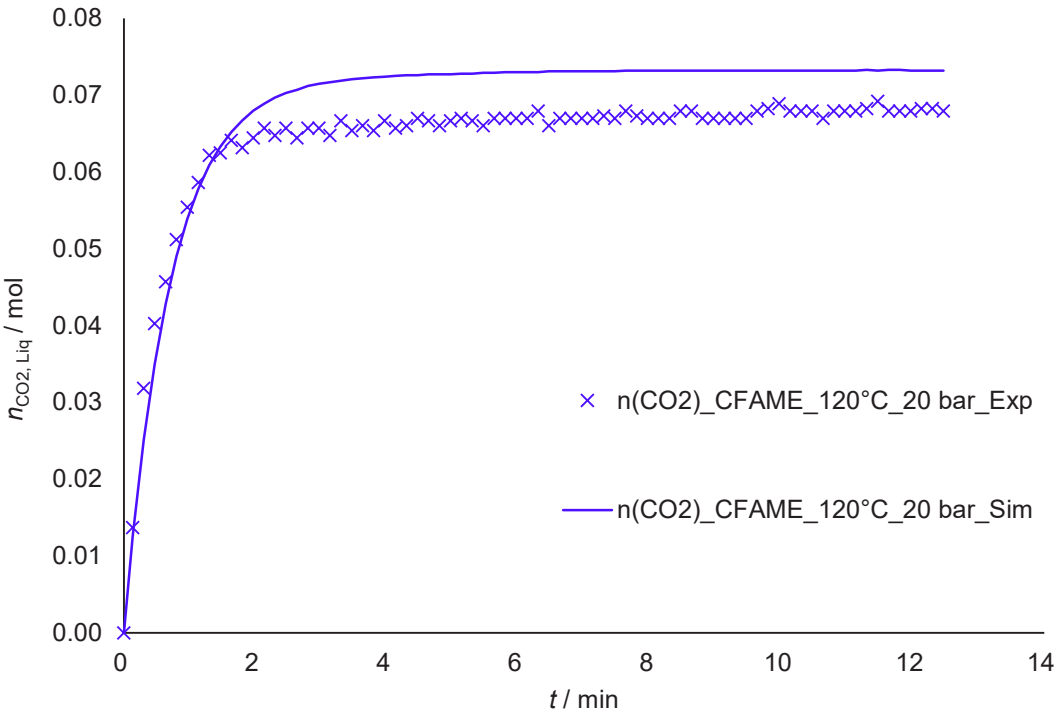

Figure S7. Kinetics of CO_2 absorption in the CFAME solution at 20 bar, 120 °C and rotating speed of 500 rpm.

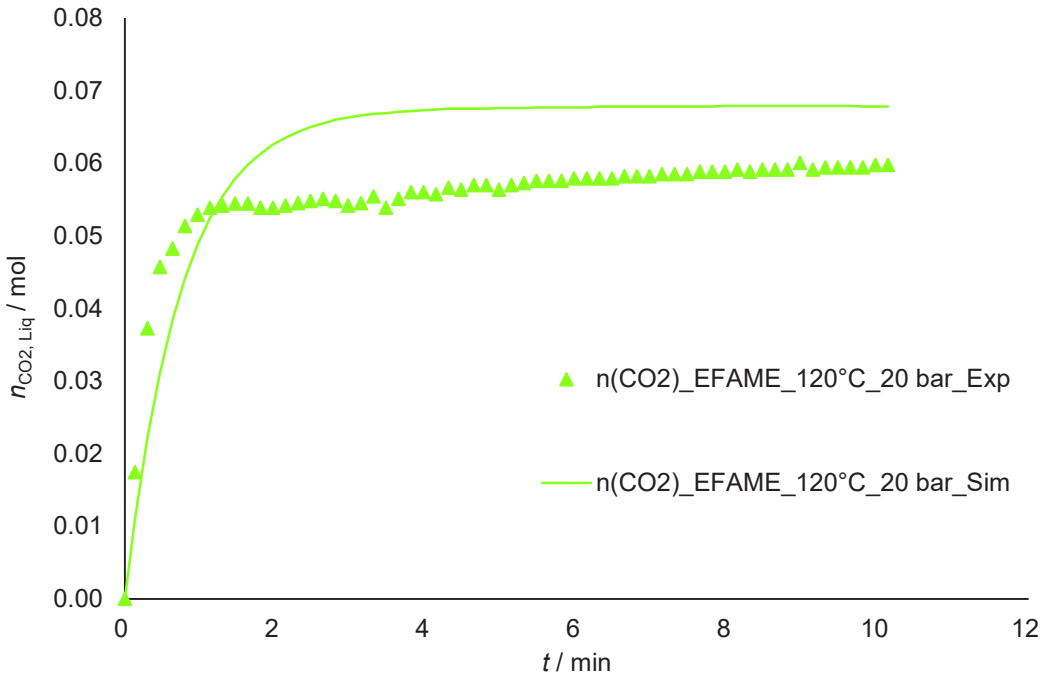

Figure S8. Kinetics of CO_2 absorption in the EFAME solution at 20 bar, 120 °C and rotating speed of 500 rpm

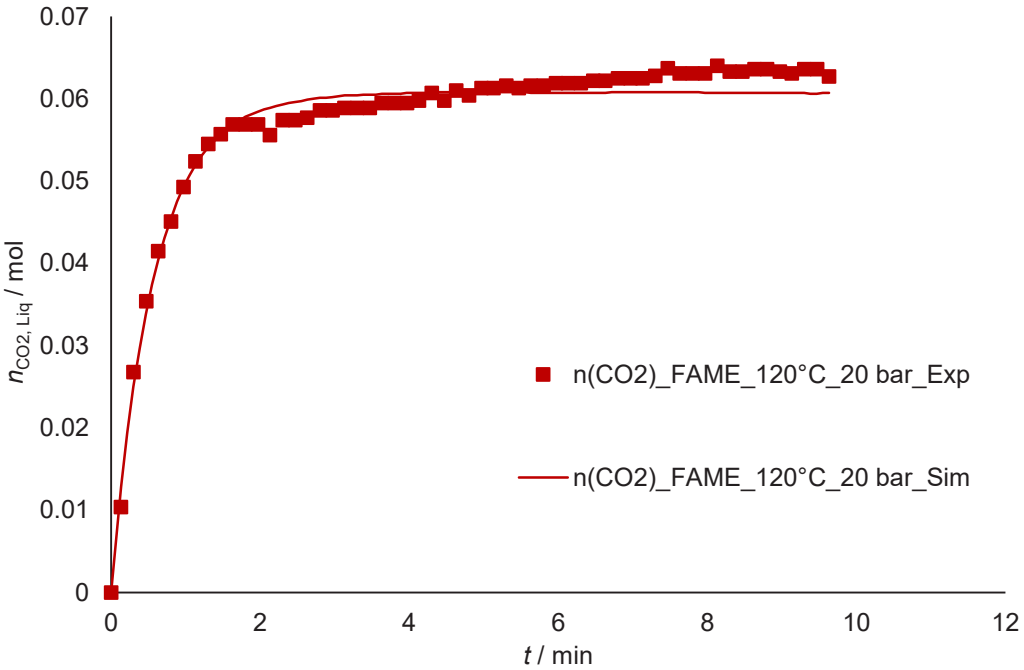

Figure S9. Kinetics of CO_2 absorption in the FAME solution at 20 bar, 120 °C and rotating speed of 500 rpm.

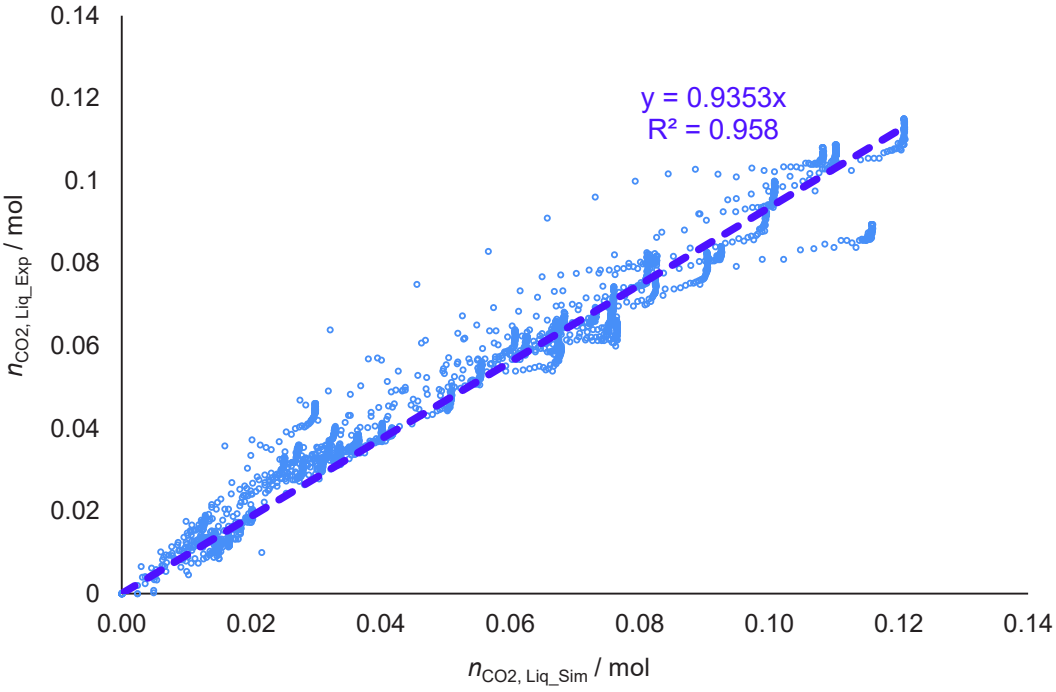

Figure S10. Overall parity plot of experimental versus simulated values for the mass transfer study

Figure S11 shows the evolution of the solubility of CO_2 in EFAME solution with the variation of CO_2 pressure. One can notice that, the solubility of CO_2 increases when the pressure increases. Also, the concentration of CO_2 follows the Henry's law at different temperature. The similar phenomenon was noticed for the FAME and CFAME (Figures S12-S13).

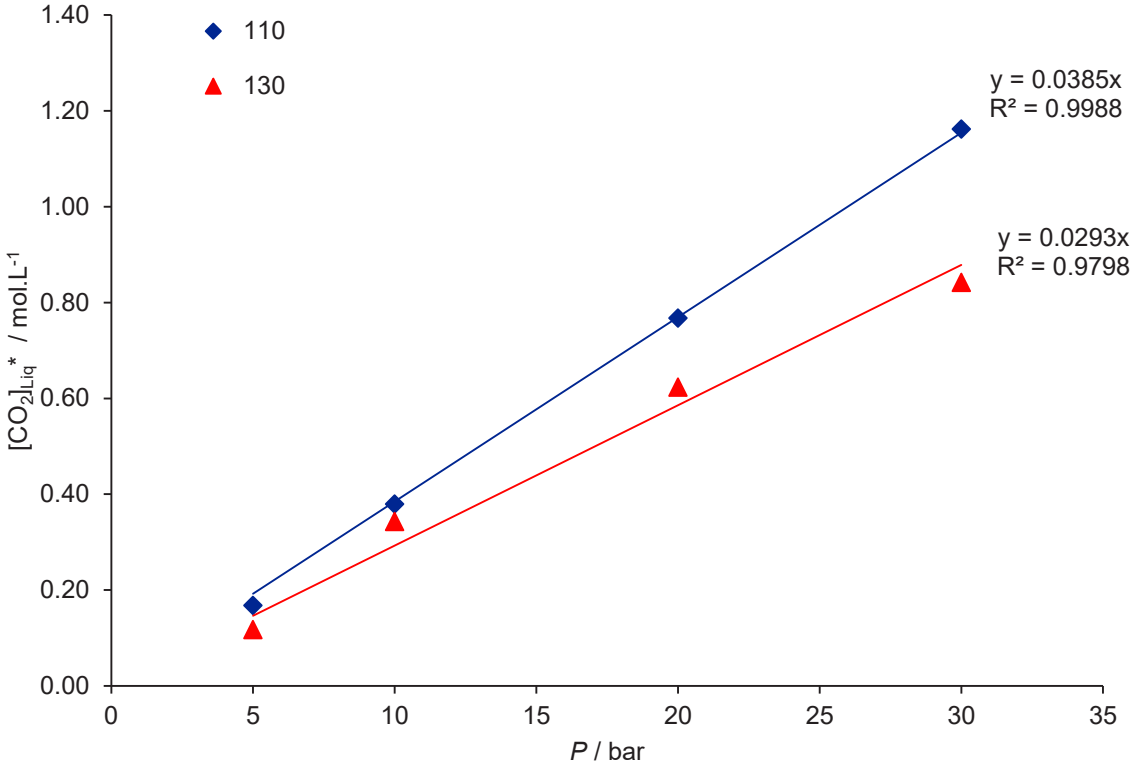

Figure S11. Evolution of the solubility of CO_2 at different CO_2 pressure for EFAME

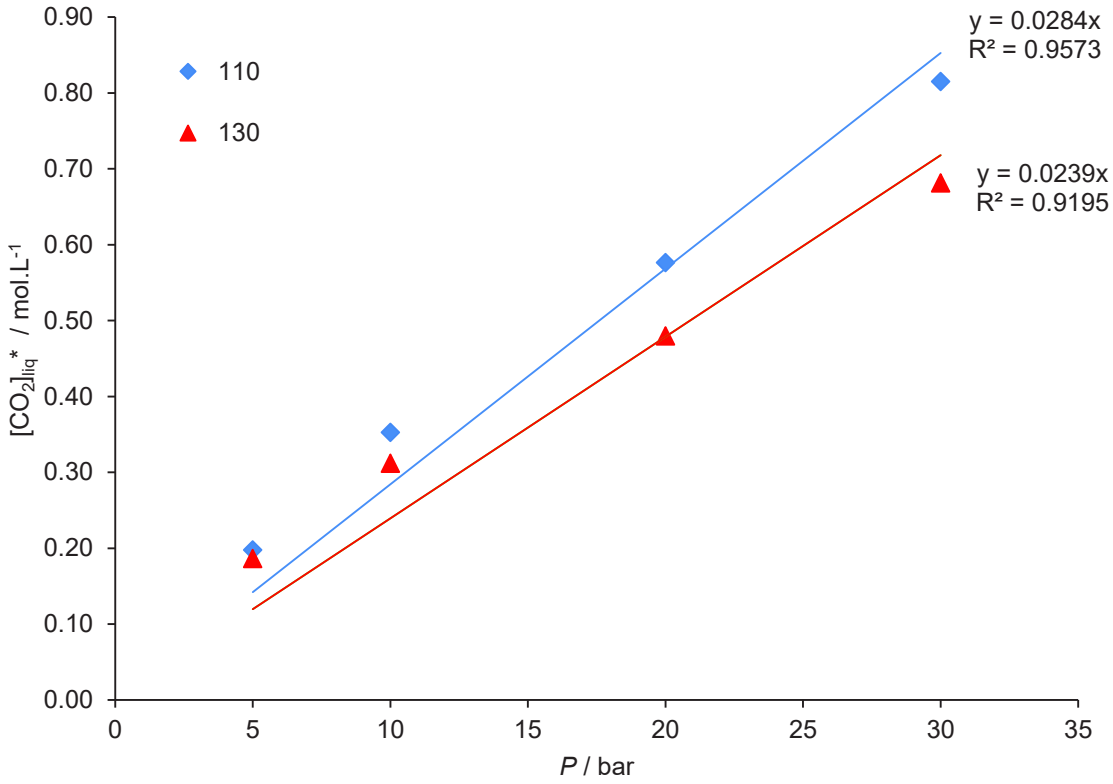

Figure S12. Evolution of the solubility of CO_2 at different CO_2 pressure for FAME

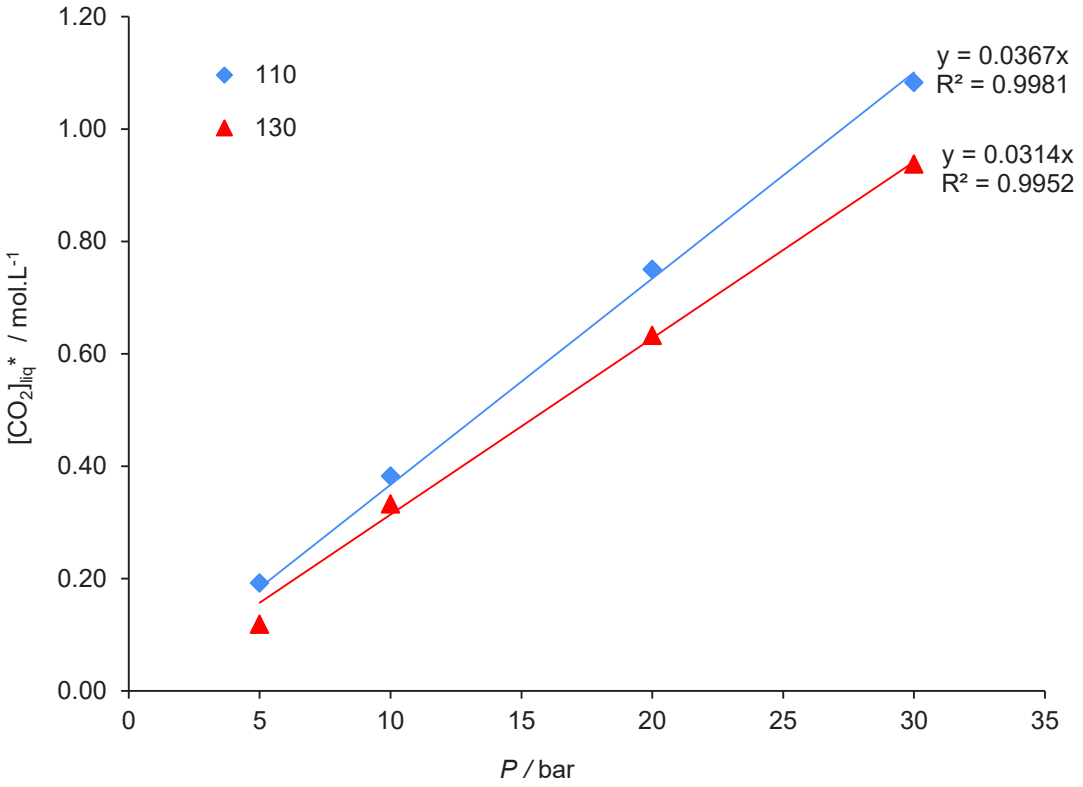

Figure S13. Evolution of the solubility of CO_2 at different CO_2 pressure for CFAME

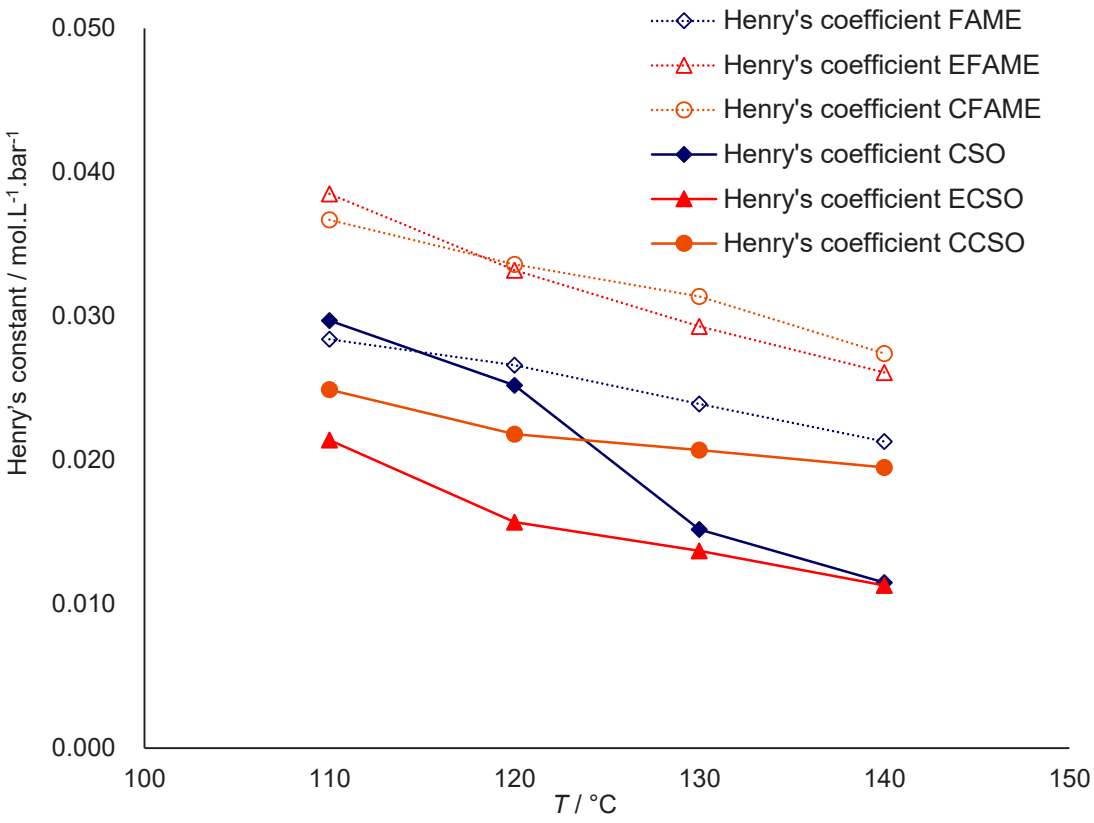

Figure S14. Evolution of the Henry's constant versus temperature

Standard deviation for the value of Henry's constant was found to be 0.0014 $mol.L^{-1}.bar^{-1}$.

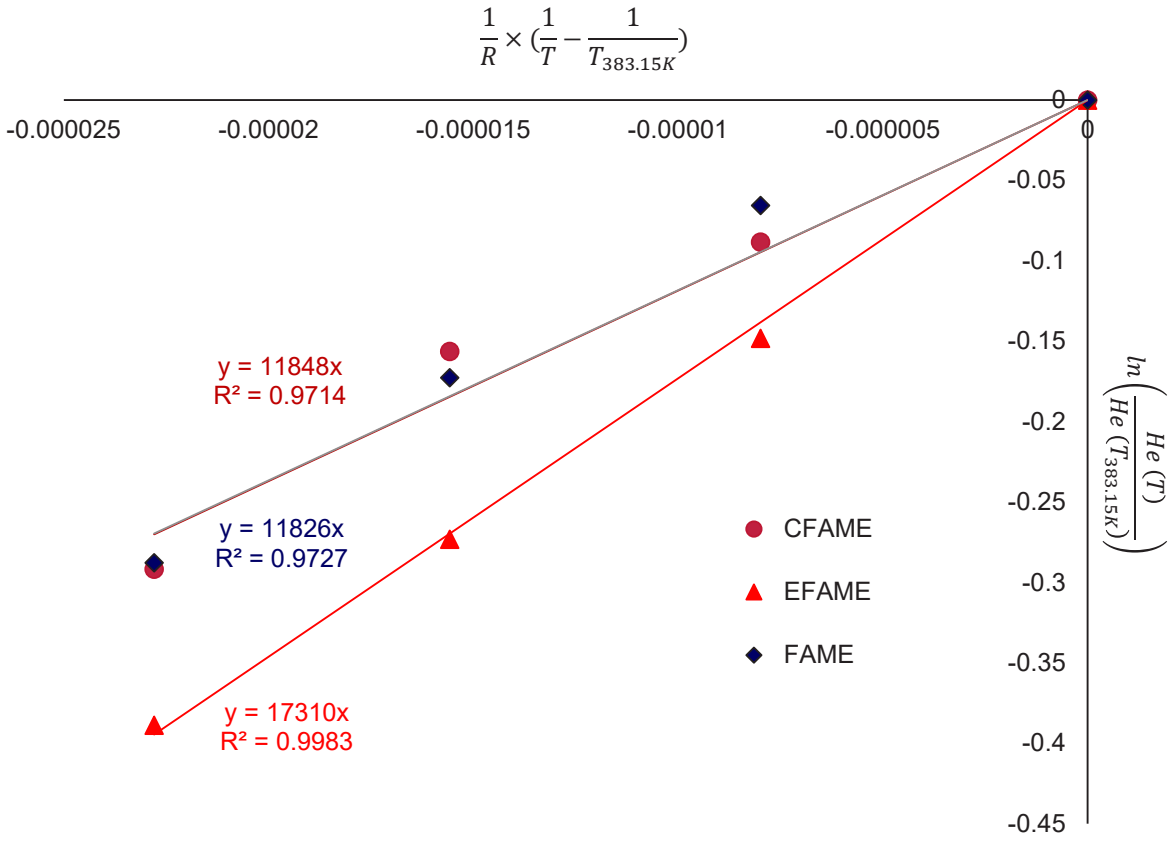

Figure S15. Van't Hoff curve for Henry's constants

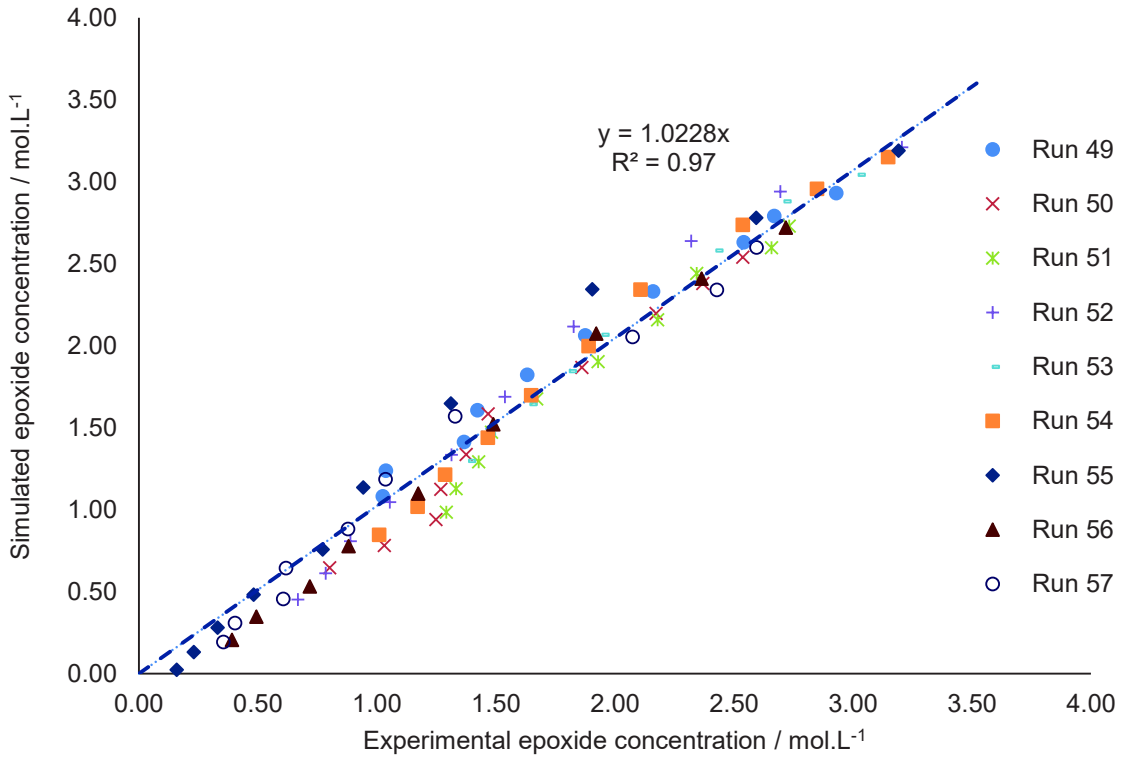

Figure S16. Overall parity plot of experimental versus simulated values for the epoxide concentration for the carbonation of EFAME.

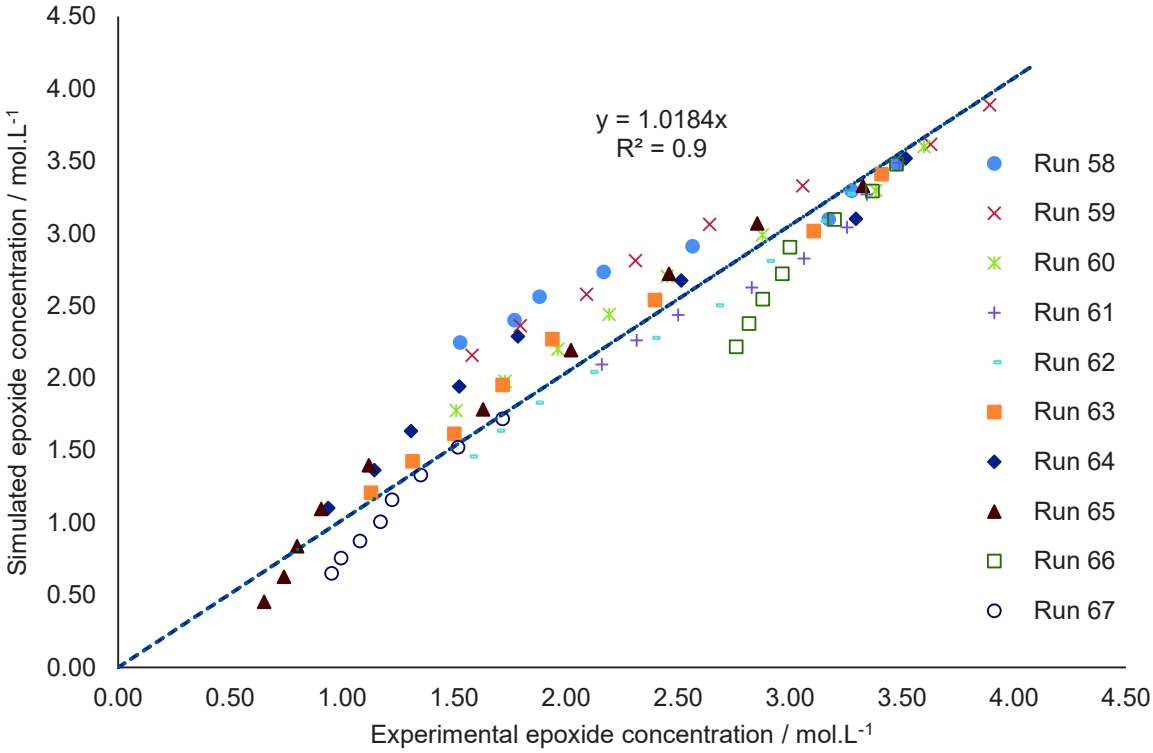

Figure S17. Overall parity plot of experimental versus simulated values for the epoxide concentration for the carbonation of ECSO.

Table S1. Mass transfer experimental matrix

Run	$P_{reactor}$ [bar]	$T_{reactor}$ [°C]	FAME [wt %]	EFAME [wt %]	CFAME [wt %]
1	5	110	100	0	0
2	5	120	100	0	0
3	5	130	100	0	0
4	5	140	100	0	0
5	10	110	100	0	0
6	10	120	100	0	0
7	10	130	100	0	0
8	10	140	100	0	0
9	20	110	100	0	0
10	20	120	100	0	0
11	20	130	100	0	0
12	20	140	100	0	0
13	30	110	100	0	0
14	30	120	100	0	0
15	30	130	100	0	0
16	30	140	100	0	0
17	5	110	0	100	0
18	5	120	0	100	0
19	5	130	0	100	0
20	5	140	0	100	0
21	10	110	0	100	0
22	10	120	0	100	0
23	10	130	0	100	0

24	10	140	0	100	0
25	20	110	0	100	0
26	20	120	0	100	0
27	20	130	0	100	0
28	20	140	0	100	0
29	30	110	0	100	0
30	30	120	0	100	0
31	30	130	0	100	0
32	30	140	0	100	0
33	5	110	0	0	100
34	5	120	0	0	100
35	5	130	0	0	100
36	5	140	0	0	100
37	10	110	0	0	100
38	10	120	0	0	100
39	10	130	0	0	100
40	10	140	0	0	100
41	20	110	0	0	100
42	20	120	0	0	100
43	20	130	0	0	100
44	20	140	0	0	100
45	30	110	0	0	100
46	30	120	0	0	100
47	30	130	0	0	100
48	30	140	0	0	100

Table S2. Experimental matrix for carbonation experiments with initial concentrations

Run	Nature of organic phase	$[Ep]_{org}$ [mol.L^{-1}]	$[DB]_{org}$ [mol.L^{-1}]	[TBAB] [mol.L^{-1}]	Pressure CO_2 [bar]	Temperature [°C]
49	EFAME	2.93	0.00	0.14	10.0	124
50	EFAME	2.54	0.00	0.14	20.0	124
51	EFAME	2.73	0.00	0.13	30.0	114
52	EFAME	3.21	0.00	0.13	33.5	130
53	EFAME	3.18	0.00	0.13	33.1	110
54	EFAME	3.15	0.00	0.13	33.0	120
55	EFAME	3.19	0.00	0.28	33.5	130
56	EFAME	2.72	0.00	0.14	30.0	140
57	EFAME	2.6	0.00	0.14	20.0	140
58	ECSO	3.48	0.00	0.13	12.0	120
59	ECSO	3.89	0.00	0.13	20.3	120
60	ECSO	3.60	0.00	0.13	30.6	120
61	ECSO	3.49	0.00	0.13	33.4	110
62	ECSO	3.41	0.00	0.13	33.8	120
63	ECSO	3.41	0.00	0.13	33.2	130
64	ECSO	3.52	0.00	0.13	20.8	140
65	ECSO	3.33	0.00	0.26	33.0	130
66	ECSO	3.48	0.00	0.03	22.4	140
67	ECSO	1.72	2.05	0.30	47.0	110

Table S3. Evolution of a' and b' for the density

	a'/kg.m^{-3}.K^{-1}	b'/kg.m^{-3}	s(θ_{mean})/%
FAME	-0.7277	1093.9	0.0690
EFAME	-0.7620	1157.8	0.0576
CFAME	-0.7309	1232.4	0.0384
CSO	-0.6736	1116.9	0.1699
ECSO	-0.6892	1182.5	0.0757
CCSO	-0.6968	1236.8	0.0432

Table S4. Arrhenius data

	A / ×10^{-7} Pa.s	*Ea* / J.mol^{-1}
FAME	45.4	-17368
EFAME	5.1	-23916
CFAME	1.8	-31203
CSO	80.0	-9402.9
ECSO	3230.0	-15979
CCSO	190.0	-27129